B7.-6

20011015 124

Summary of

Drag Coefficients

of

Various Shaped Cylinders

C. F. Heddleson
D. L. Brown
R. T. Cliffe

File

① Fluid Dynamic Drag, Cylinders

② Cylinders, Fluid Dynamic Drag

③ Aerodynamic Drag, Cylinders

AIRCRAFT NUCLEAR PROPULSION DEPARTMENT
ATOMIC PRODUCTS DIVISION

GENERAL ⊛ ELECTRIC

LEGAL NOTICE

Summary of Drag Coefficients of
Various Shaped Cylinders

C. F. Heddleson
D. L. Brown
R. T. Cliffe

APRIL, 1957

GENERAL ⚡ ELECTRIC

ATOMIC PRODUCTS DIVISION
AIRCRAFT NUCLEAR PROPULSION DEPARTMENT
Cincinnati 15, Ohio

Abstract

Data are presented which can be used to predict the aerodynamic drag force caused by cylinders having different cross-sectional shapes. Drag characteristics of circular, square, rectangular, triangular, diamond, and elliptical cylinders, as well as a large range of thickness-to-chord ratio symmetrical airfoil shapes, are presented as a function of Reynolds number. In addition, certain Mach number characteristics are discussed.

Contents

Symbols

A_f Body frontal projected area normal to flow direction

A_L Body lateral projected area parallel to flow direction

a   Speed of sound

b   Frontal width of cylinder

b_o Frontal width of basic cylinder without rounded corners

c   Streamwise dimensions of cylinder or chord

C_D Drag coefficient, $\dfrac{\text{Drag force on cylinder}}{\text{Area (q)}}$

$(C_D)_{std}$ Standard drag coefficient at a standard Reynolds number

c_o Chord (parallel to flow) of basic cylinder without rounded corners

D   Drag force

FR   Fineness ratio, c_o/b_o

f   Frequency of vortex discharge from one side of cylinder

L   Length of cylinder axis

M   Free-stream Mach number, V/a

M_{cr} Critical Mach number; the free-stream speed at which the velocity at some point on the surface of a cylinder reaches the local speed of sound

q   Free-stream dynamic pressure, $1/2 \, V^2$

Re   Reynolds number, $\rho \, \dfrac{Vc}{\mu}$

$(Re)_{std}$ Standard Reynolds number (8,000,000) used for extrapolation of drag coefficients

r   Cross-sectional corner radius of cylinder

V   Free-stream velocity

b_o/c_o Thickness ratio of cylinder

r/b_o Cross-sectional corner-radius ratio of cylinder

$f\,b/V$ Strouhal number

ρ Density of air, $slugs/ft^3$

μ Absolute viscosity of air, $lb\text{-}sec/ft^2$

Introduction

Data has been collected from available literature on the aerodynamic characteristics of various cylindrical streamline shapes. These data can be used for the prediction of the over-all drag of a single tube, and comparisons can be made between tubes of different shapes. Both Reynolds number effects and Mach number effects are considered.

As a solid body moves through a fluid, a certain amount of resistance is encountered by the body; and conversely, as a fluid flows past a solid body, the fluid encounters resistance. This resistance to the movement of a solid in a liquid is known as drag, this drag being brought about by the shear stresses exerted in the boundary layer of the fluid next to the solid surface. If the boundary layer is completely laminar in character, then the shear forces are viscous forces alone; but if the boundary layer is turbulent, the resistance results from velocity fluctuation in the fluid of the boundary layer. These resistances are surface drag. However, when separation of the boundary layer occurs, the fluid immediately behind the body is in turbulent motion. This turbulent wake results in loss of energy in addition to that lost owing to surface drag. This loss of energy due to the turbulent wake is form drag and is a function of the form or shape of the body past which the fluid is flowing.

The coefficient of friction, or the coefficient of drag, for flow past solid bodies is defined in the same way as the friction factor for circular tubes, i. e.,

$$D = \frac{C_D \rho V^2 A}{2}$$

where D is the force of resistance exerted on the body due to fluid flow past it, and A is either the frontal or lateral projected area, depending upon the particular data correlation. It is important to distinguish upon which area the drag coefficient is based. Usually thin streamline struts are evaluated on lateral projected area, whereas cylinders and bodies of revolution are based on frontal projected area in a plane normal to the flow.

The coefficient of drag is a function of Reynolds number, Mach number, angle of attack, and form of the body. When the force is calculated from the coefficient of drag, it includes both the surface and form drag. The drag coefficient used to calculate the resisting force to flow is the same whether the flow is past the body or the body is moving through the fluid. [6]

Only the zero lift (zero angle of attack) conditions are being considered. Minimum drag normally occurs at zero lift, which, consequently, will be the condition of most interest.

Heat transfer coefficients and drag of tube banks have not been included; however, a survey of available literature on flow over tube banks is included to aid in the design of tube banks for heat exchangers. The prediction of the resistance to flow of fluids over tube banks is difficult since interference must be considered when tubes are in proximity to each other. For this reason the drag of a single tube is not in general the same as that of an individual tube within a tube bank.

Circular Cylinders

Much material has been published concerning flow over circular cylinders. A typical presentation of drag coefficient of a circular cylinder is shown in Figure 1. Comparison of the values of the drag coefficients for a circular cylinder, as shown by the dotted line and test points in Figure 1, indicates sizable differences for subcritical Reynolds numbers (Re = 1.3×10^4 to 2.5×10^5). This difference in the drag coefficient was due to end flow effects for the test points shown. Therefore, a better value of drag can be obtained by using the dotted curve between Re 1.3×10^4 to 2.5×10^5. The drag and Reynolds number for a circular cylinder are calculated as follows.

$$D = \frac{C_D \rho V^2 A_F}{2}$$

$$Re = \frac{V_c \rho}{\mu}$$

A breakdown of total drag for a circular cylinder into form drag and surface drag is presented in Figure 2. Except at Re = 10 and 20 the form drag was predicted from measurements of normal pressure, and the skin-friction drag was taken as the difference between the total drag and the form drag. The skin-friction and form drags at Re = 10 and 20 were determined from a numerical solution of the equations for the flow of a viscous fluid around a cylinder. The figure shows that at Re = 10 the contribution of the skin friction amounts to about 43 per cent of the total drag; the contribution then falls with increasing Reynolds number and becomes quite small at Re = 10^4. A broken line in the figure shows that the skin-friction drag over the range $30 < Re < 10^4$ is closely given by the relation $C_D = 4Re^{-1/2}$.

The data of Knudsen and Katz[6] for the variation of drag coefficient with varying cylinder length-to-diameter ratio at a Reynolds number of 88,000 is presented in Table 1. A plot of these data on log-log paper will be a straight line. The equation of this drag coefficient curve at a Reynolds number of 88,000 is

$$C_D = \frac{1}{4.55} \; (2.85 \div \text{Log } L/c)$$

Also shown in Figure 1 is the variation of Strouhal number, f b/V, with Reynolds number. This number is an indication of the frequency of vortex discharge from one side of a cylinder. Accompanying this discharge of vortices from the cylinder is a fluctuation of the pressure in the wake.

Data presented in this report are only for isolated cylinders and should not be added together for the resultant drag for a bank of tubes. The flow in the wake behind a cylinder is usually quite different from the flow upstream; therefore, interference effects must be considered when cylinders are in close proximity to each other or to walls. As a matter of interest, the relative drag of two wires in tandem is shown in Figure 3. For a complete study of tube banks the bibliography at the end of this report should be consulted.

9

TABLE 1

EFFECT OF THE LENGTH-TO-DIAMETER RATIO FOR

FLOW PAST CIRCULAR CYLINDERS

(Knudsen & Katz)

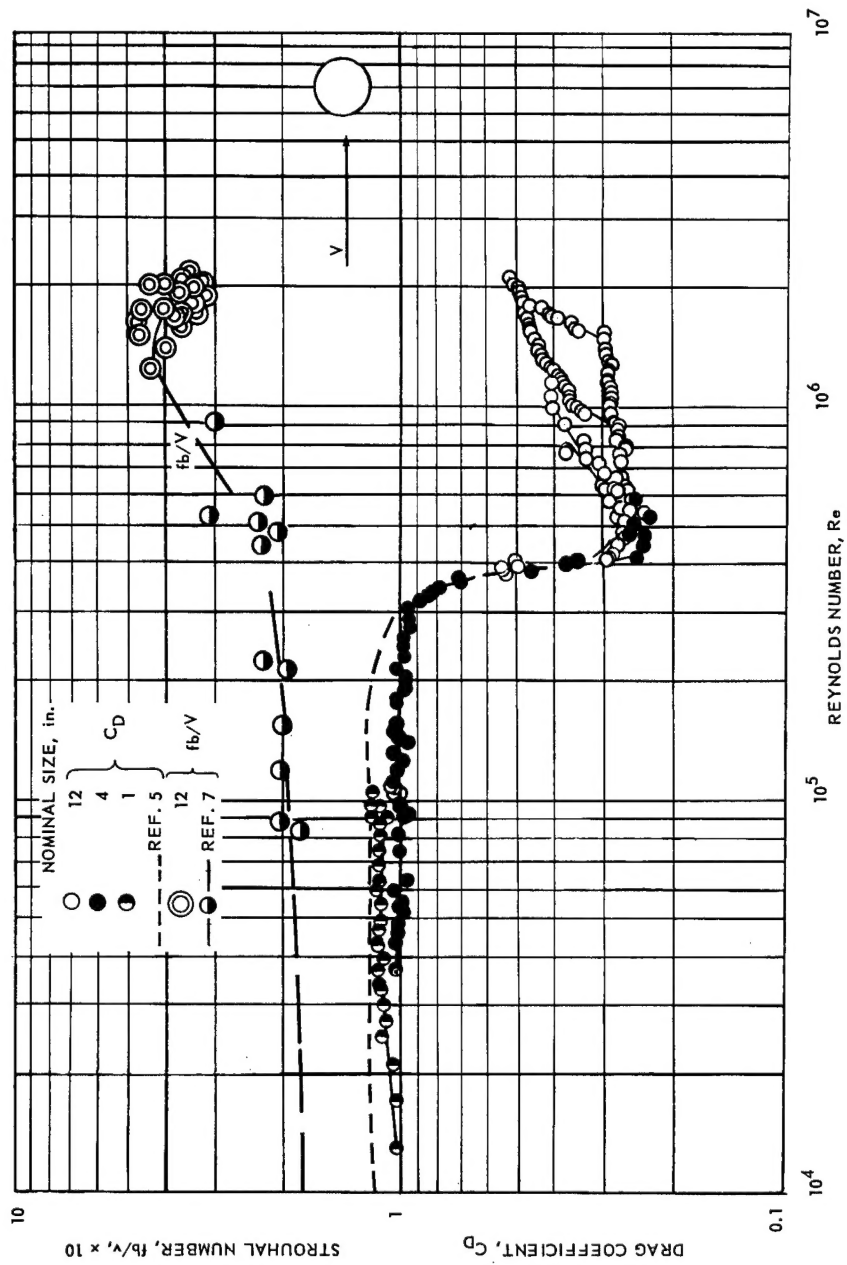| Fluid Dynamics and Heat Transfer	
$\text{Re} = 88,000$	
$\left(\dfrac{L/b_0}{\text{Infinity}} \right)$	$\left(\dfrac{C_D}{1.2} \right)$
40	0.98
20	0.92
10	0.82
5	0.74
3	0.74
2	0.68
1	0.63

Fig. 1 – Variation of drag coefficients and strouhal number with Reynolds number for circular cylinders (NACA-TN-3038)
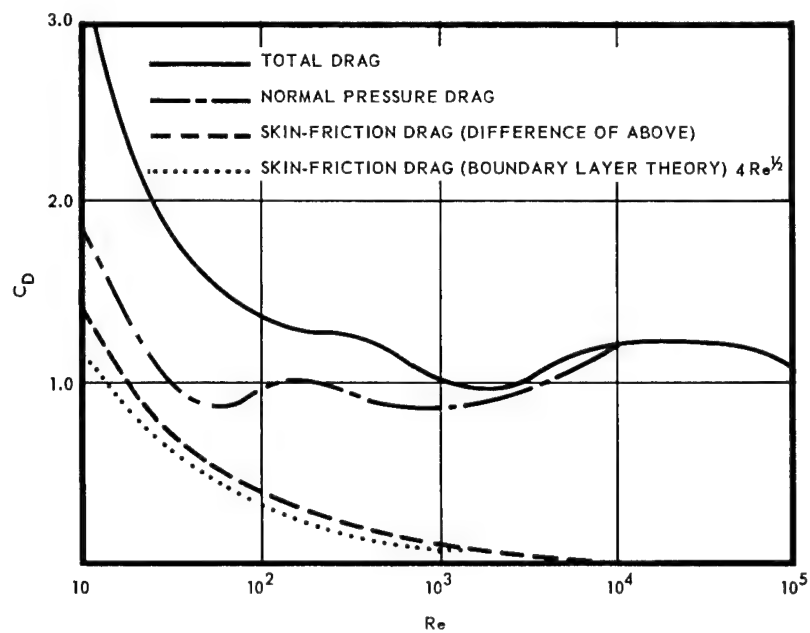
Fig. 2 — Contribution of skin friction to the total drag of a circular cylinder (Modern Developments in Fluid Dynamics)
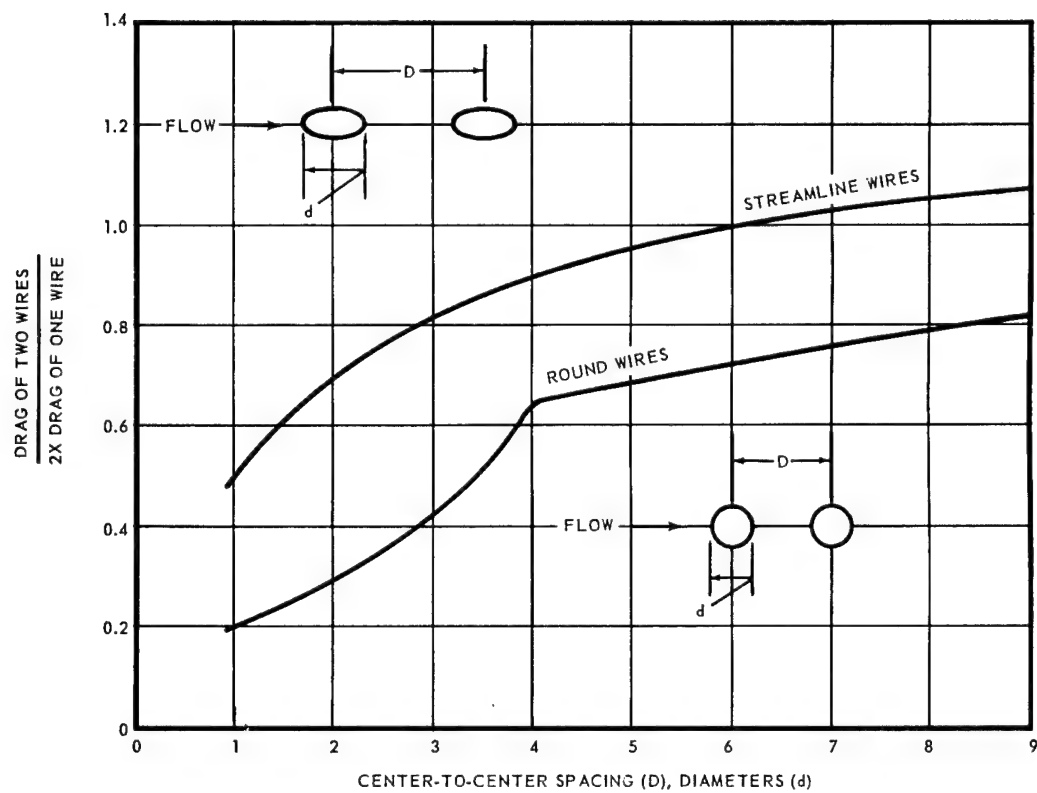

Fig. 3 — Relative drag of small wires in combination

Elliptical Cylinders

The drag and Reynolds number of elliptical cylinders can be calculated using the following expressions.

$$D = C_D \frac{A_L \rho V^2}{2}$$

$$Re = \frac{Vc\rho}{\mu}$$

The resistance provided by an elliptical cylinder is considerably less than that provided by a circular cylinder. The effect of streamlining the rear portion of a solid body results in cutting down considerably the turbulent wake behind the body. This results in a reduction of the drag coefficient past these solid bodies.

The data on ellipses by Lindsey[14] and by Delany and Sorensen[9] are combined in Figure 4. In general, the drag coefficient decreases with decreasing thickness ratio (tube thickness to chord ratio). At higher Reynolds numbers the drag coefficients of the two thin elliptic cylinders (25% and 12.5% chord) are seen to increase suddenly, whereas the other cylinders show decreasing drag coefficients. This rapid rise in drag coefficient is due to compressibility effects at the higher velocities. Two curves are shown for the ellipse with a thickness ratio of 50 per cent chord corresponding to two sources which used models of different dimensions. Both curves are of the same characteristic shape, and the differance can be attributed to scale effect.[16] These curves indicate the relative values of the drug coefficients of ellipses compared to the drag coefficient of a circular cylinder. For example, at a value of $Re = 10^5$ an ellipse with a thickness of 12.5 per cent chord has a resistance less than 1/5 that of a circular cylinder of the same thickness.

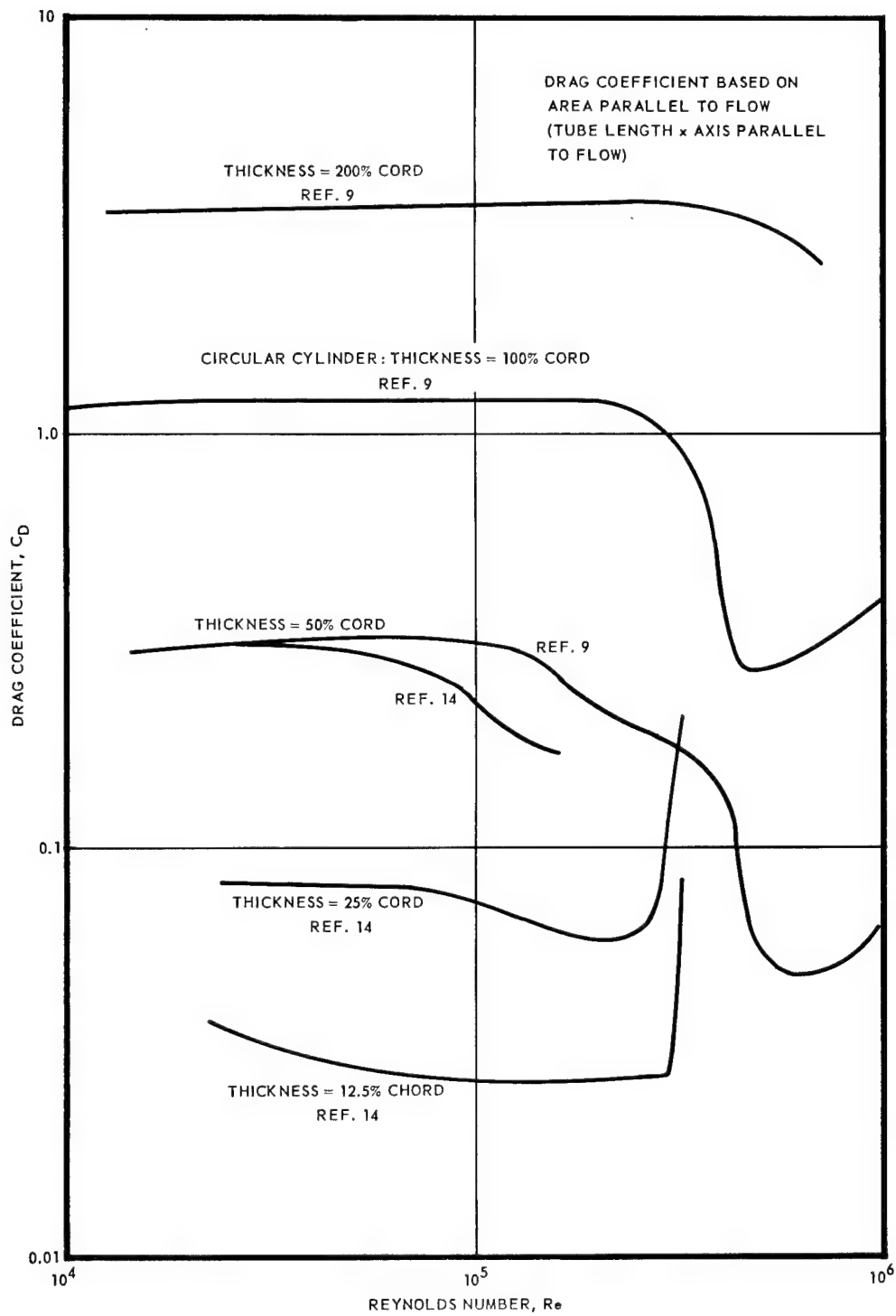Data are also presented in Figure 13. However, These are based on A_F rather than A_L.

Fig. 4 — Effect of thickness ratio on drag characteristics of ellipses

Triangular Cylinders

The effect of the apex angle on the drag coefficient of triangular cylinders is shown in Figure 5. Four isosceles triangles are presented in this figure with angles of attack of 0° (apex into the airstream) and 180° (base into the airstream). As might be expected, the drag is lower for the case of the cylinders having their apex into the airstream, and the drag coefficient decreases with decreasing apex angle.

The variation of drag coefficient with Mach number for the triangular cylinders is shown in Figure 6. From these data it is not possible to determine exactly the critical Mach number. However, the curve for the cylinder with a 30° apex angle and base into the airstream seems to break sharply upward at a Mach number of slightly over 0.7, indicating that this may be the critical Mach number. The critical Mach number is defined as that free-stream speed at which sonic velocity is reached at some point on the surface of the body.

The drag and Reynolds numbers are calculated as follows:

$$D = C_D \frac{V^2 \rho A_F}{2}$$

$$Re = \frac{Vc\rho}{\mu}$$

Additional data showing the effect of rounding the corners on triangular cylinders are presented in Figure 20 and 21. It should be noted that the drag coefficient here is also based on A_F.
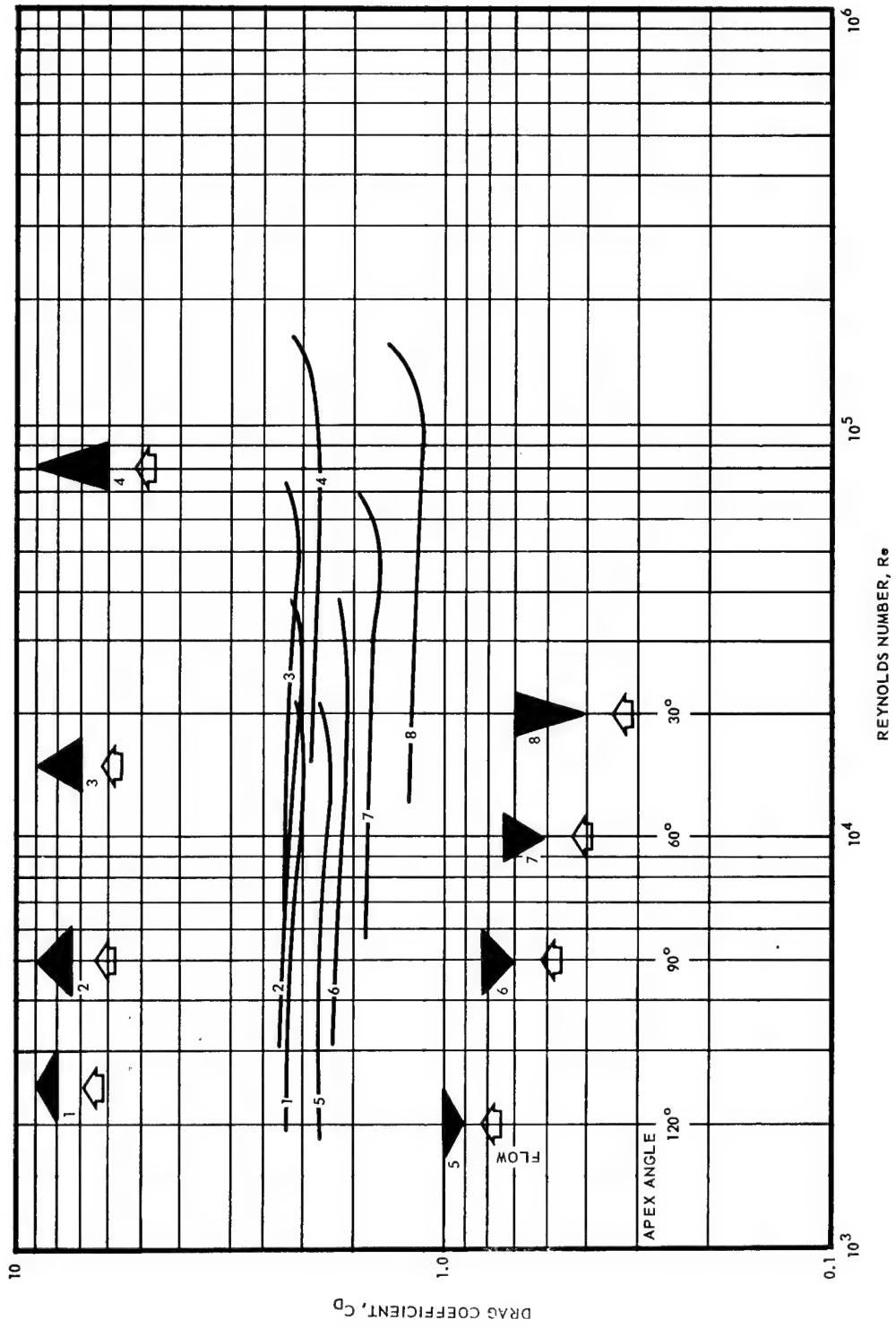
15

16

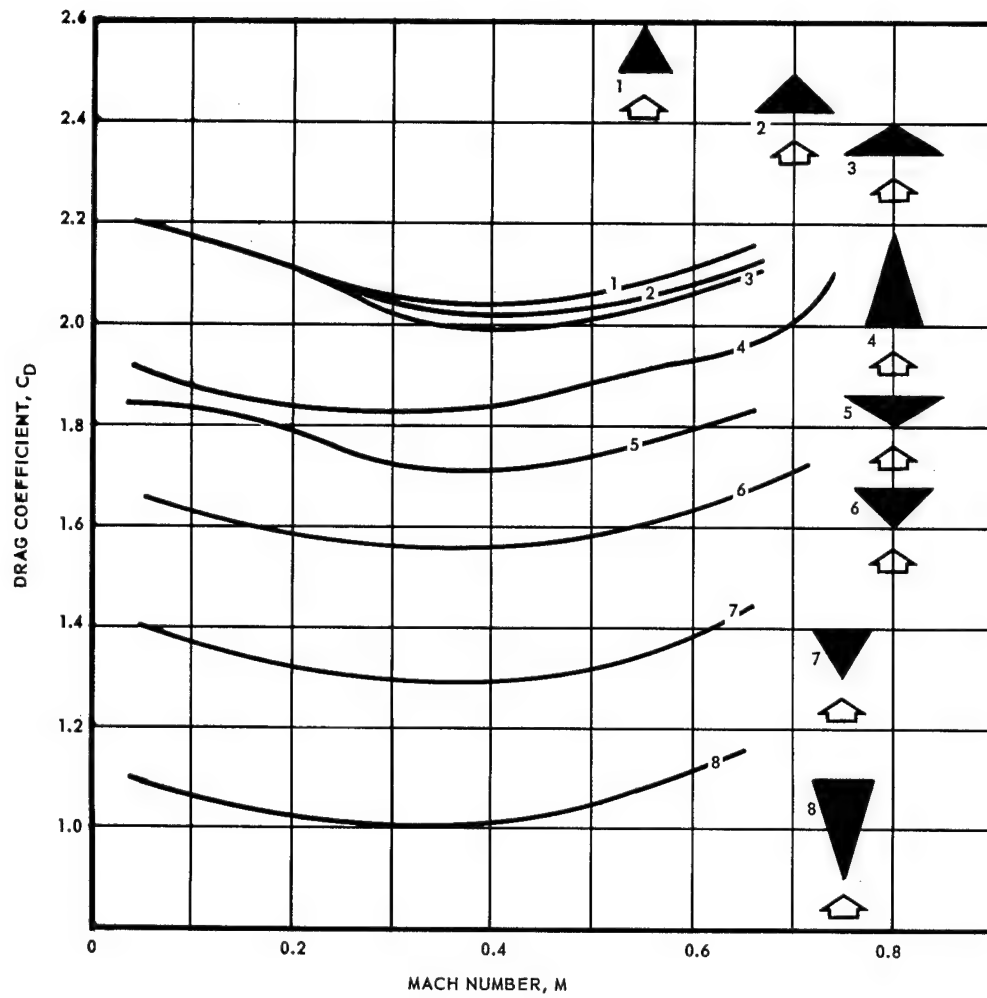Fig. 5 — Variation of drag coefficient with Reynolds number for triangular cylinders

Fig. 6—Variation of drag coefficient with Mach number for triangular cylinders

Symmetrical Airfoils

The variation of drag coefficient with Reynolds number for a family of airfoil sections with thickness ratios from nine to eighteen per cent of the chord is shown in Figure 7. Also presented in this figure is the theoretical drag coefficient variation of flat plates. It can be seen that the general shape of the drag coefficient curves for the airfoil sections follows a pattern similar to the "laminar-transition-turbulent" flow curve of the flat plate. However, at the lower Reynolds numbers the airfoil curves do not exhibit a uniform pattern. At higher Reynolds numbers (3,000,000 and above) the drag coefficient curves show a definite relationship. Reference 16 presents the following extrapolation formula:

$$C_D = (C_D)_{std} \left[\frac{(Re)_{std}}{Re} \right]^{0.11}$$

where $(C_D)_{std}$ is the standard airfoil-section drag coefficient at a standard Reynolds, $(Re)_{std}$, of about 8,000,000. For aerodynamically smooth airfoils extrapolations to a higher Reynolds number using this formula are considered reasonably conservative.

Figure 8 presents the drag coefficient variation with Reynolds number for families of symmetrical airfoil sections (Tables 2 through 7 give the ordinates of these sections). These airfoil sections are grouped by thickness ratio on the plot. Similar lines show the sections which are related by leading-edge shape. The drag and Reynolds number can be calculated from the following relations

$$D = C_D \frac{V^2 \rho}{2} AL$$

$$Re = \frac{Vc\rho}{\mu}$$

The airfoil sections presented here are all NACA-designated shapes. Reference 17 explains in detail how these shapes were designed. The last two numbers in any of these NACA-series numbers is the maximum thickness in per cent of the chord. The 00-series airfoils are some of the basic symmetrical sections with the maximum thickness located at 30 per cent of the chord behind the leading edge. In the 6-series designations the second number is the position of the minimum pressure in tenths of the chord behind the leading edge. The subscript following this number, if any, gives the range of lift coefficients in tenths above and below the design lift coefficient in which favorable pressure gradients exist on both surfaces. Following the dash is the design lift coefficient in tenths.

It should be noted that drag coefficients shown in Figure 7 are somewhat lower than those for the same designation shown in Figure 8. The data for Figure 7[17] has been corrected for turbulence within the wind tunnel where the tests were made and should be considered optimum. The airfoil sections in both figures were aerodynamically smooth (polished surfaces). Airfoil sections with standard roughness on the surfaces will have considerably higher drag coefficients (Figure 9). A complete description of smooth and rough airfoils

19

is given in Reference 17. Airfoil shapes constructed by normal methods are usually between the aerodynamically smooth and standard-roughness airfoils, and the drag coefficients are also between these limits.

The dependence of drag on the thickness parameter, which is here taken to be the ratio of the maximum thickness b to the chord length c, is best illustrated by comparative measurements on sections belonging to the same family. The family of symmetrical sections shown in Figure 10 was derived from a circle by conformal transformation of the generalized Joukowski type. The coordinates for the shapes shown in Figure 10 are tabulated in Table 8.

A curve is given in Figure 11 showing the change in C_D (drag per unit length/$(1/2 \rho V^2 c)$, where V is the undisturbed stream velocity) with b/c, at a Reynolds number Vc/μ equal to 4×10^5. C_D increases with b/c, at first slowly and then more rapidly. The curve must become steeper at values of b/c greater than those shown, since there is reason to believe that when b/c = 1, C_D has a value differing only slightly from its value for a circular cylinder. This value (for the same Reynolds number) is 0.32, so the rise in C_D over the range $0.4 < b/c < 1.0$ must be from 0.033 to about 10 times this value.

It should be noted that the drag coefficients in Figure 11 are based on A_L. Drag coefficient data for the same airfoils are presented in Figure 12 as a function of surface area.

In practice it is often necessary to fair a bluff cylindrical obstacle. If the thickness is denoted by b, the strut which will have the lowest drag is one for which the drag coefficient obtained by dividing the drag per unit length by $1/2 \rho V^2 b$ is a minimum. This drag coefficient (at Re = 4×10^5) for several thickness ratios is plotted in Figure 13. The section with the lowest drag coefficient is one whose chord length is about three to four times the thickness. If a greater chord length is taken, the increase in the skin-friction drag more than compensates for the slight drop in form drag, whereas if a smaller chord length is taken, the drop in the skin-friction drag is smaller than the rise in the form drag.

The above reasoning applies, as indicated, to obtain minimum pressure loss for a given thickness. Other application such as heat transfer may dictate smaller thickness ratios from a heat transfer area consideration. It is suggested that separate analysis be made for these special applications.

In Table 9 data are presented for design of struts with thickness ratios varying from 20 to 40 per cent.

Drag coefficients of the various shapes depend on both Reynolds number and Mach number. At low air velocities the Reynolds number almost entirely determines the flow pattern around a body. As the air velocity increases, the compressibility effects become more important and, ultimately, become so large that Reynolds number effects may be neglected for first approximations. The free-stream speed at which the velocity at some point on the surface of the airfoil reaches the local speed of sound is referred to as the critical speed or critical Mach number, M_{cr}. Figure 14 shows the variation of critical Mach number with maximum thickness for families of NACA symmetrical airfoils. This variation is compared to the critical Mach number variation of elliptic cylinders in Figure 15. Increasing the Mach number beyond the critical value will cause an extreme rise in the drag coefficient as shown in Figure 4.

TABLE 2

SYMMETRICAL AIRFOIL COORDINATES - SIX PER CENT THICKNESS
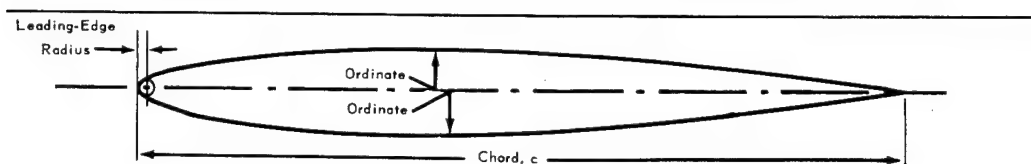
Six Per Cent Thickness

NACA Airfoil Section	0006	63-006	64-006	65-006	66-006
Station, % Chord	Ordinates, % Chord				
0	0	0	0	0	0
0.5	--	0.503	0.494	0.476	0.461
0.75	--	0.609	0.596	0.574	0.544
1.25	0.95	0.771	0.754	0.717	0.693
2.5	1.31	1.057	1.024	0.956	0.918
5.0	1.78	1.462	1.405	1.310	1.257
7.5	2.10	1.766	1.692	1.589	1.524
10	2.34	2.010	1.928	1.824	1.752
15	2.67	2.386	2.298	2.197	2.119
20	2.87	2.656	2.572	2.482	2.401
25	2.97	2.841	2.772	2.697	2.618
30	3.00	2.954	2.907	2.852	2.782
35	--	3.000	2.981	2.952	2.899
40	2.90	2.971	2.995	2.998	2.971
45	--	2.877	2.919	2.983	3.000
50	2.65	2.723	2.775	2.900	2.985
55	--	2.517	2.575	2.741	2.925
60	2.68	2.267	2.331	2.518	2.915
65	--	1.982	2.050	2.246	2.611
70	1.83	1.670	1.740	1.935	2.316
75	--	1.342	1.412	1.594	1.953
80	1.31	1.008	1.072	1.233	1.543
85	--	0.683	0.737	0.865	1.107
90	0.72	0.383	0.423	0.510	0.665
95	0.40	0.138	0.157	0.195	0.267
100	0	0	0	0	0
Leading-Edge Radius	0.40	0.297	0.256	0.240	0.223

TABLE 3

SYMMETRICAL AIRFOIL COORDINATES - NINE PER CENT THICKNESS

NACA Airfoil Section[a]	0009	63-009	64-009	65-009	66-009
Station, % Chord	Ordinates, % Chord				
0	0	0	0	0	0
0.5	--	0.749	0.739	0.700	0.687
0.75	--	0.906	0.892	0.845	0.824
1.25	1.42	1.151	1.128	1.058	1.030
2.5	1.96	1.582	1.533	1.421	1.368
5.0	2.67	2.196	2.109	1.961	1.880
7.5	3.15	2.655	2.543	2.383	2.283
10	3.51	3.024	2.898	2.736	2.626
15	4.01	3.591	3.455	3.299	3.178
20	4.30	3.997	3.868	3.727	3.601
25	4.46	4.275	4.170	4.050	3.927
30	4.50	4.442	4.373	4.282	4.173
35	--	4.500	4.479	4.431	4.348
40	4.35	4.447	4.490	4.496	4.457
45	--	4.296	4.364	4.469	4.499
50	3.97	4.056	4.136	4.336	4.475
55	--	3.739	3.826	4.086	0.381
60	3.42	3.358	3.452	3.743	4.204
65	--	2.928	3.026	3.328	3.882
70	2.75	2.458	2.561	2.856	3.428
75	--	1.966	2.069	2.342	2.877
80	1.97	1.471	1.564	1.805	2.263
85	--	0.990	1.069	1.260	1.611
90	1.09	0.550	0.611	0.738	0.961
95	0.60	0.196	0.227	0.280	0.374
100	0	0	0	0	0
Leading-Edge Radius	0.89	0.631	0.579	0.552	0.530

[a]See Table 2 for sketch

TABLE 4

SYMMETRICAL AIRFOIL COORDINATES - TWELVE PER CENT THICKNESS

NACA Airfoil Section[a]	63_1-012	64_1-012	65_1-012	66_1-012
Station, % Chord		Ordinates, % Chord		
0	0	0	0	0
0.5	0.985	0.978	0.923	0.906
0.75	1.194	1.179	1.109	1.087
1.25	1.519	1.490	1.387	1.358
2.5	2.102	2.035	1.875	1.808
5.0	2.925	2.810	2.606	2.496
7.5	3.542	3.394	3.172	3.037
10	4.039	3.871	3.647	3.496
15	4.799	4.620	4.402	4.234
20	5.342	5.173	4.975	4.801
25	5.712	5.576	5.406	5.238
30	5.930	5.844	5.716	5.568
35	6.000	5.978	5.912	5.803
40	5.920	5.981	5.997	5.947
45	5.704	5.798	5.949	6.000
50	5.370	5.480	5.757	5.965
55	4.935	5.056	5.412	5.836
60	4.420	4.548	4.943	5.588
65	3.840	3.974	4.381	5.139
70	3.210	3.350	3.743	4.515
75	2.556	2.695	3.059	3.767
80	1.902	2.029	2.345	2.944
85	1.274	1.382	1.630	2.083
90	0.707	0.786	0.947	1.234
95	0.250	0.288	0.366	0.474
100	0	0	0	0
Leading-Edge Radius	1.087	1.040	1.000	0.952

[a]See Table 2 for sketch

TABLE 5

SYMMETRICAL AIRFOIL COORDINATES - FIFTEEN PER CENT THICKNESS

NACA Airfoil Section[a]	63_2-015	64_2-015	65_2-015	66_2-015
Station, % Chord	Ordinates, % Chord			
0	0	0	0	0
0.5	1.204	1.208	1.124	1.122
0.75	1.462	1.456	1.356	1.343
1.25	1.878	1.842	1.702	1.675
2.5	2.610	2.528	2.324	2.235
5.0	3.648	3.504	3.245	3.100
7.5	4.427	4.240	3.959	3.781
10	5.055	4.842	4.555	4.358
15	6.011	5.785	5.504	5.286
20	6.693	6.480	6.223	5.995
25	7.155	6.985	6.764	6.543
30	7.421	7.319	7.152	6.956
35	7.500	7.482	7.396	7.250
40	7.386	7.473	7.498	7.430
45	7.099	7.224	7.427	7.495
50	6.665	6.810	7.168	7.450
55	6.108	6.266	6.720	7.283
60	5.453	5.620	6.118	6.959
65	4.721	4.895	5.403	6.372
70	3.934	4.113	4.600	5.576
75	3.119	3.296	3.744	4.632
80	2.310	2.472	2.858	3.598
85	1.541	1.677	1.977	2.530
90	0.852	0.950	1.144	1.489
95	0.300	0.346	0.428	0.566
100	0	0	0	0
Leading-Edge Radius	1.594	1.590	1.505	1.435

[a]See Table 2 for sketch

TABLE 6

SYMMETRICAL AIRFOIL COORDINATES - EIGHTEEN PER CENT THICKNESS

NACA Airfoil Section[a]	63₃-018	64₃-018	65₃-018	66₃-018
Station, % Chord		Ordinates, % Chord		
0	0	0	0	0
0.5	1.404	1.428	1.337	1.323
0.75	1.713	1.720	1.608	1.571
1.25	2.217	2.177	2.014	1.952
2.5	3.104	3.005	2.751	2.646
5.0	4.362	4.186	3.866	3.690
7.5	5.308	5.076	4.733	4.513
10	6.068	5.803	5.457	5.210
15	7.225	6.942	6.606	6.333
20	8.048	7.782	7.476	7.188
25	8.600	8.391	8.129	7.848
30	8.913	8.789	8.595	8.346
35	9.000	8.979	8.886	8.701
40	8.845	8.952	8.999	8.918
45	8.482	8.630	8.901	8.998
50	7.942	8.114	8.568	8.942
55	7.256	7.445	8.008	8.733
60	6.455	6.658	7.267	8.323
65	5.567	5.782	6.395	7.580
70	4.622	4.842	5.426	6.597
75	3.650	3.866	4.396	5.451
80	2.691	2.888	3.338	4.206
85	1.787	1.951	2.295	2.934
90	0.985	1.101	1.319	1.714
95	0.348	0.400	0.490	0.646
100	0	0	0	0
Leading-Edge Radius	2.120	2.208	1.960	1.955

[a]See Table 2 for sketch

TABLE 7

SYMMETRICAL AIRFOIL COORDINATES - TWENTY-ONE PER CENT THICKNESS

NACA Airfoil Section[a]	634-021	644-021	654-021	664-021
Station, % Chord	Ordinates, % Chord			
0	0	0	0	0
0.5	1.583	1.646	1.522	1.525
0.75	1.937	1.985	1.838	1.804
1.25	2.527	2.517	2.301	2.240
2.5	3.577	3.485	3.154	3.045
5.0	5.065	4.871	4.472	4.269
7.5	6.182	5.915	5.498	5.233
10	7.080	6.769	6.352	6.052
15	8.441	8.108	7.700	7.369
20	9.410	9.095	8.720	8.376
25	10.053	9.807	9.487	9.153
30	10.412	10.269	10.036	9.738
35	10.500	10.481	10.375	10.154
40	10.298	10.431	10.499	10.407
45	9.854	10.030	10.366	10.500
50	9.206	9.404	9.952	10.434
55	8.390	8.607	9.277	10.186
60	7.441	7.678	8.390	9.692
65	6.396	6.649	7.360	8.793
70	5.290	5.549	6.224	7.610
75	4.160	4.416	5.024	6.251
80	3.054	3.287	3.800	4.796
85	2.021	2.213	2.598	3.324
90	1.113	1.245	1.484	1.924
95	0.392	0.449	0.546	0.717
100	0	0	0	0
Leading-Edge Radius	2.650	2.884	2.500	2.550

[a]See Table 2 for sketch

TABLE 8

CONTOURS OF JOUKOWSKI SECTIONS ORDINATES ABOVE AND BELOW THE CENTER-

LINE OF EACH SECTION. ALL DIMENSIONS EXPRESSED AS FRACTIONS OF THE

CHORD LENGTH

	SECTION						
Distance from nose	1	2	3	4	5	6	7
0	0	0	0	0	0	0	0
0.025	0.0107	0.0205	0.0295	0.0390	0.0564	0.0660	0.0808
0.050	0.0152	0.0288	0.0413	0.0566	0.0764	0.0916	0.1116
0.100	0.0205	0.0388	0.0559	0.0776	0.1027	0.1221	0.1500
0.150	0.0238	0.0452	0.0650	0.0900	0.1182	0.1428	0.1753
0.200	0.0259	0.0490	0.0705	0.0976	0.1291	0.1548	0.1904
0.250	0.0270	0.0513	0.0741	0.1014	0.1341	0.1613	0.2000
0.30	0.0275	0.0520	0.0753	0.1034	0.1364	0.1635	0.2014
0.35	0.0275	0.0520	0.0751	0.1028	0.1359	0.1630	0.2014
0.40	0.0270	0.0506	0.0733	0.1000	0.1327	0.1602	0.2000
0.45	0.0261	0.0489	0.0703	0.0966	0.1282	0.1548	0.1945
0.50	0.0250	0.0461	0.0662	0.0910	0.1218	0.1466	0.1856
0.55	0.0235	0.0430	0.0617	0.0845	0.1136	0.1362	0.1733
0.60	0.0214	0.0393	0.0559	0.0772	0.1032	0.1243	0.1596
0.65	0.0196	0.0352	0.0499	0.0686	0.0900	0.1112	0.1438
0.70	0.0172	0.0307	0.0433	0.0590	0.0773	0.0975	0.1253
0.75	0.0150	0.0260	0.0365	0.0497	0.0645	0.0817	0.1055
0.80	0.0126	0.0210	0.0293	0.0397	0.0514	0.0654	0.0842
0.85	0.0100	0.0161	0.0219	0.0293	0.0386	0.0485	0.0623
0.90	0.0074	0.0113	0.0151	0.0200	0.0260	0.0316	0.0411
0.95	0.0048	0.0064	0.0086	0.0103	0.0141	0.0158	0.0212
1.0	0.	0.	0.	0.	0.	0.	0.
Radius at nose	0.0024	0.0088	0.0189	0.0359	0.0636	0.0905	0.1384
Radius at tail	0.0024	0.0024	0.0025	0.0024	0.0027	0.0027	0.0034

TABLE 9

SYMMETRICAL AIRFOIL COORDINATES –
TWENTY TO FORTY PER CENT THICKNESS[20]
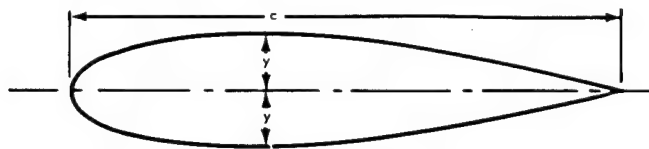
STATION, % Chord	y % Chord
0	0
1.25	26.0
2.50	37.1
5.00	52.5
7.50	63.6
10.00	72.0
12.50	78.5
15.00	83.6
17.50	87.8
20.00	91.1
25.00	95.9
30.00	98.8
35.00	100.0
40.00	99.5
45.00	97.0
50.00	95.0
55.00	91.0
60.0	86.1
65.0	80.1
70.0	73.2
75.0	65.3
80.0	56.2
85.0	46.1
90.0	33.8
95.0	19.0
100.0	0.0
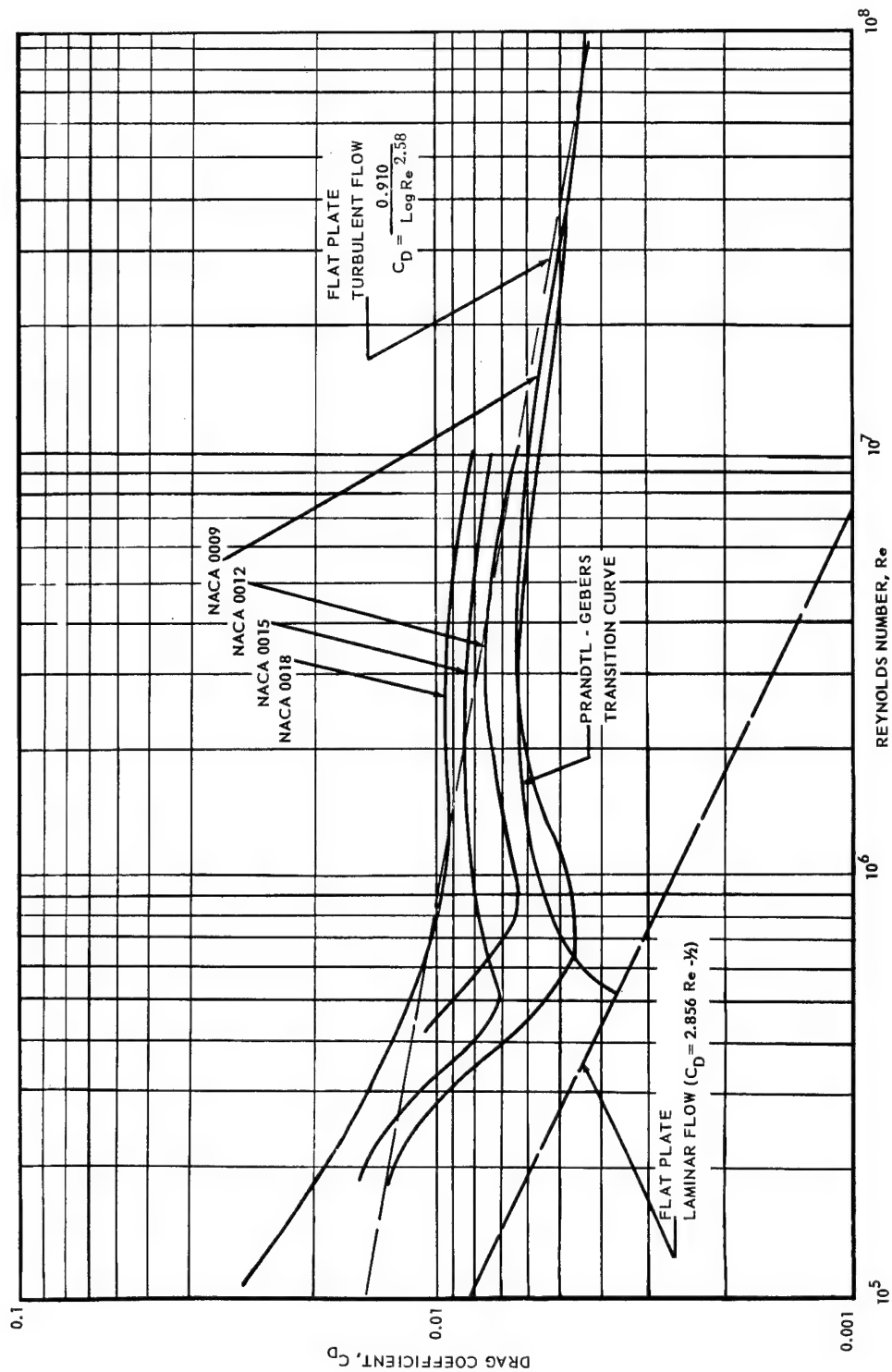
Fig. 7.— Variation of minimum drag coefficient with Reynolds number (NACA 586)

30
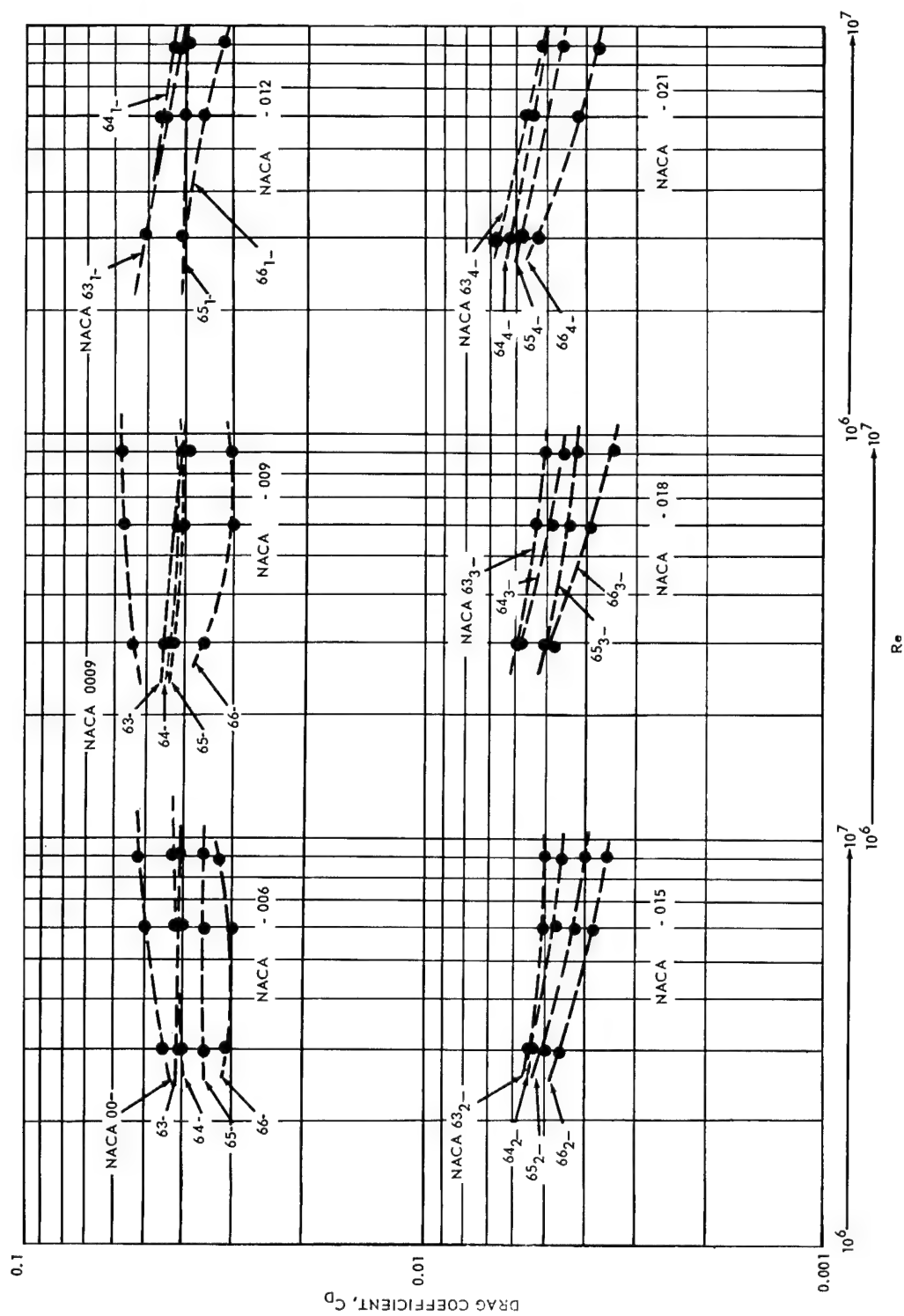
Fig. 8 — Variation of drag coefficient with Reynolds number for a family of symmetrical airfoils

31
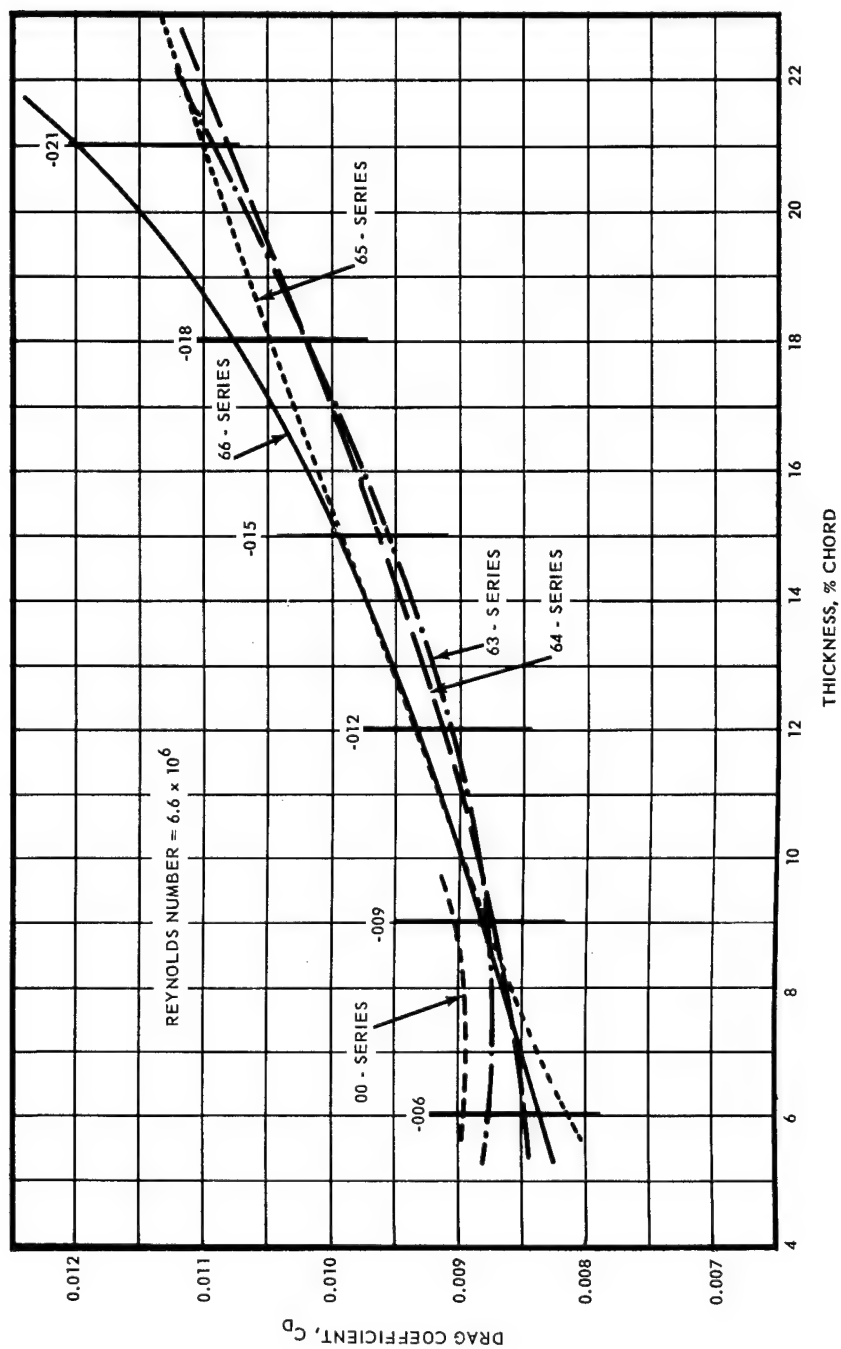
Fig. 9 – Variation of minimum drag coefficient with thickness for symmetrical NACA airfoils with standard surface roughness

THICKNESS RATIO, b/c

SECTION 1

0.0551

2

0.1040

3

0.1506

4

0.2069

5

0.2726

6

0.3270

7

0.4025
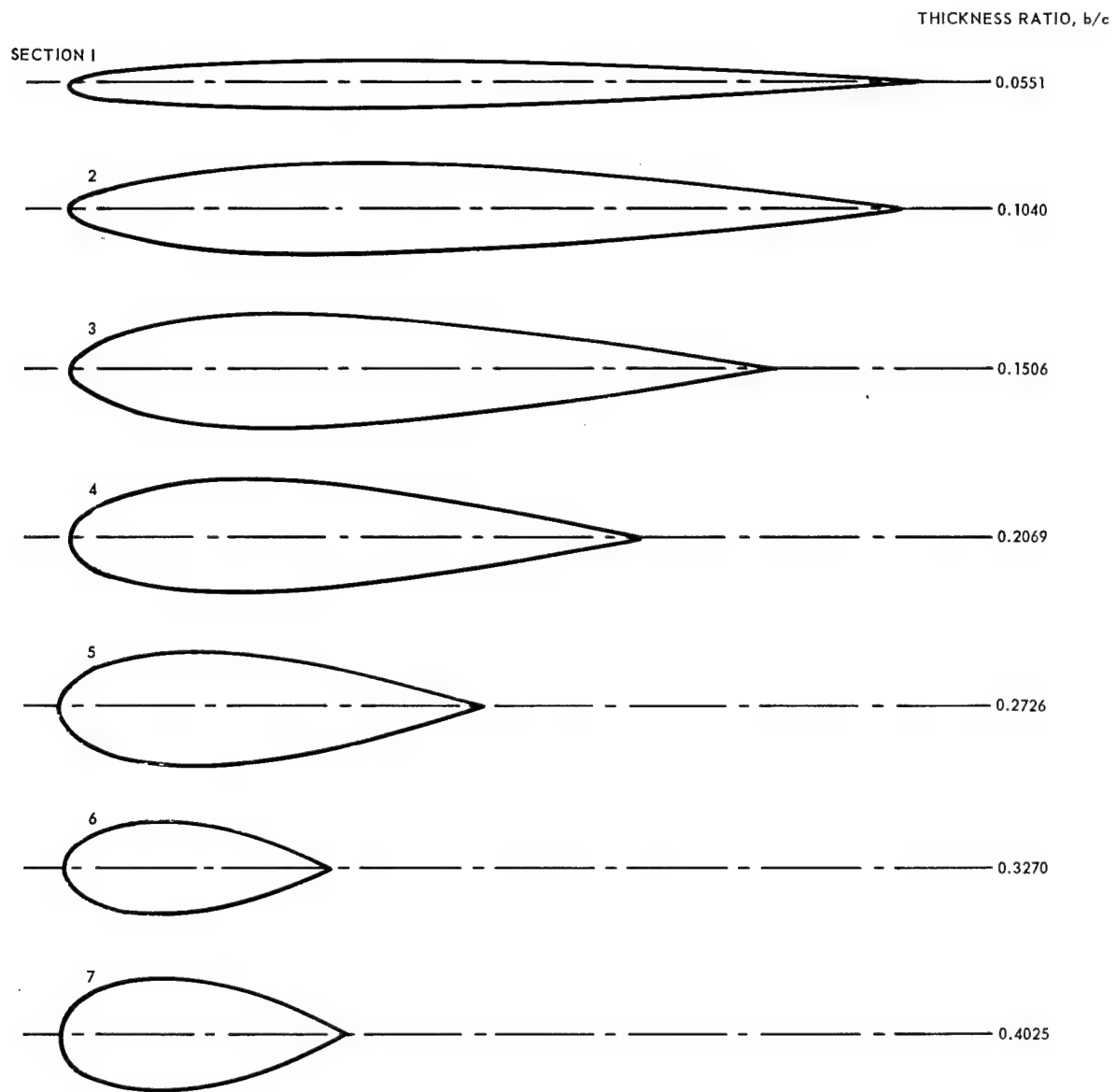
Fig. 10 – Joukowski sections
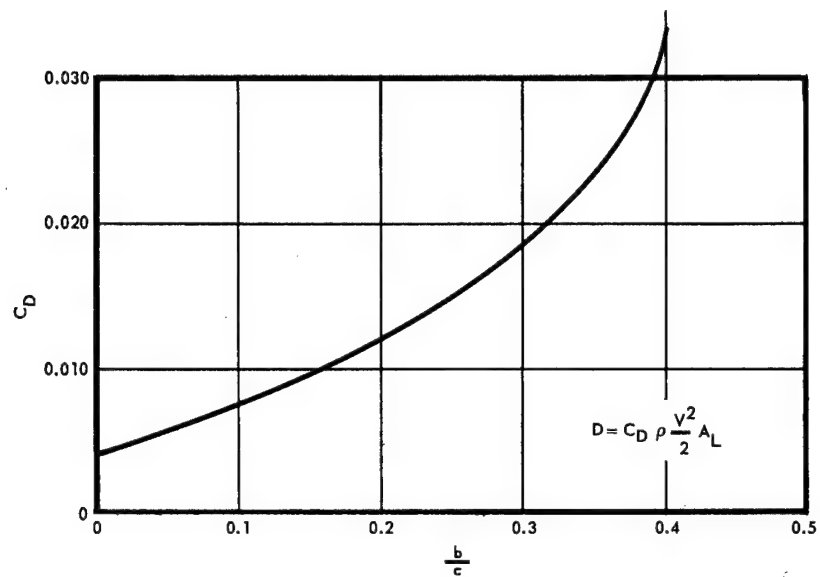
Fig. 11 — Variation of drag coefficient with thickness ratio for symmetrical airfoils

34
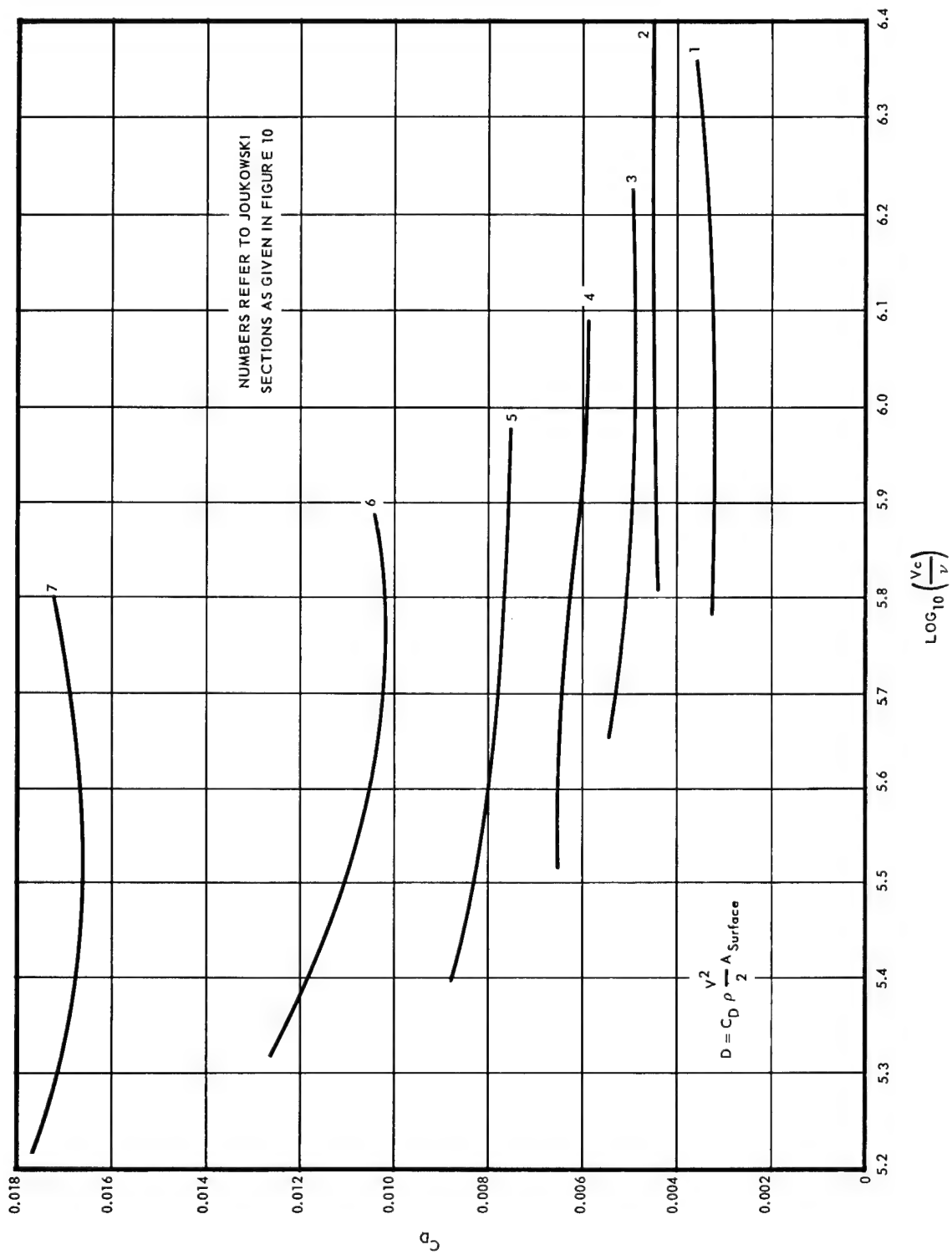
Fig. 12 – Drag coefficients of Joukowski sections
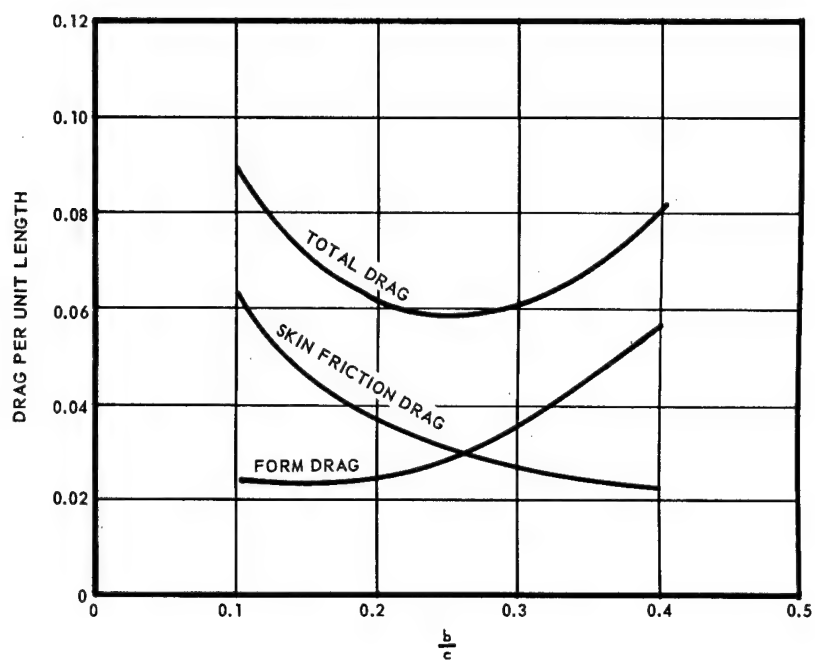
Fig. 13 — Variation of drag per unit length with thickness ratio for symmetrical airfoils
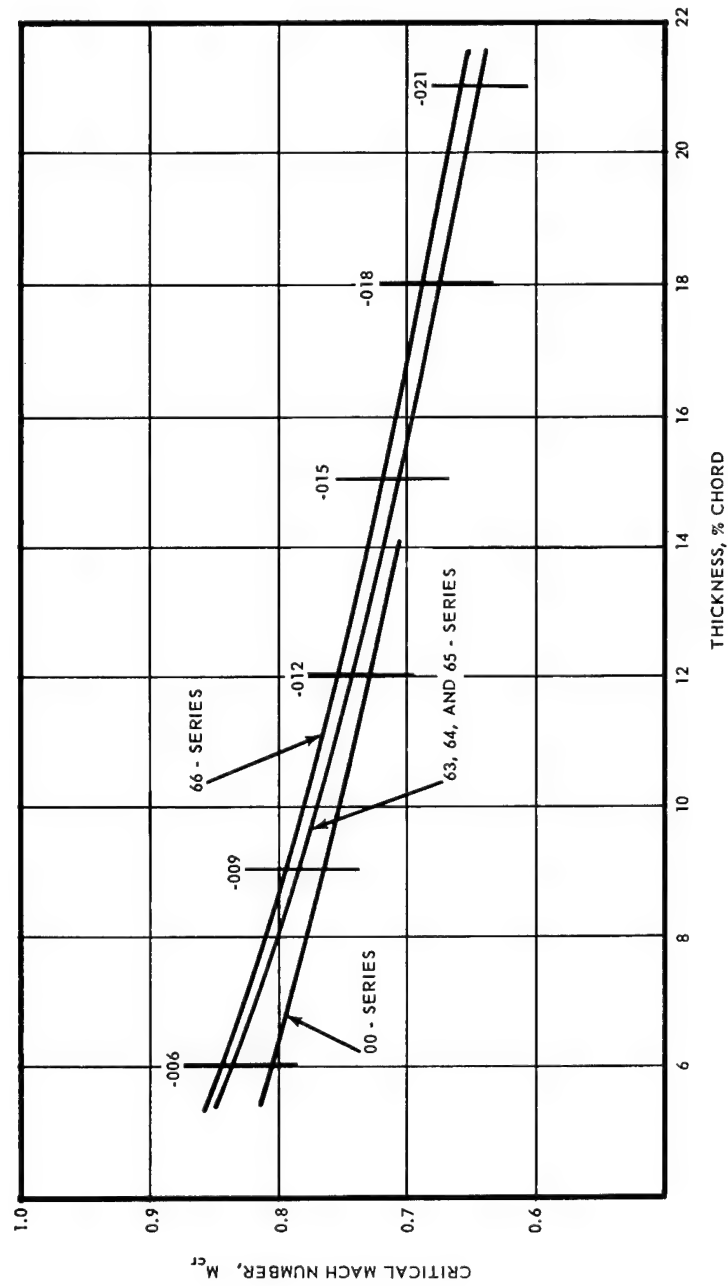
Fig. 14 — Variation of critical Mach number with thickness for airfoil families at zero lift (NACA 824)
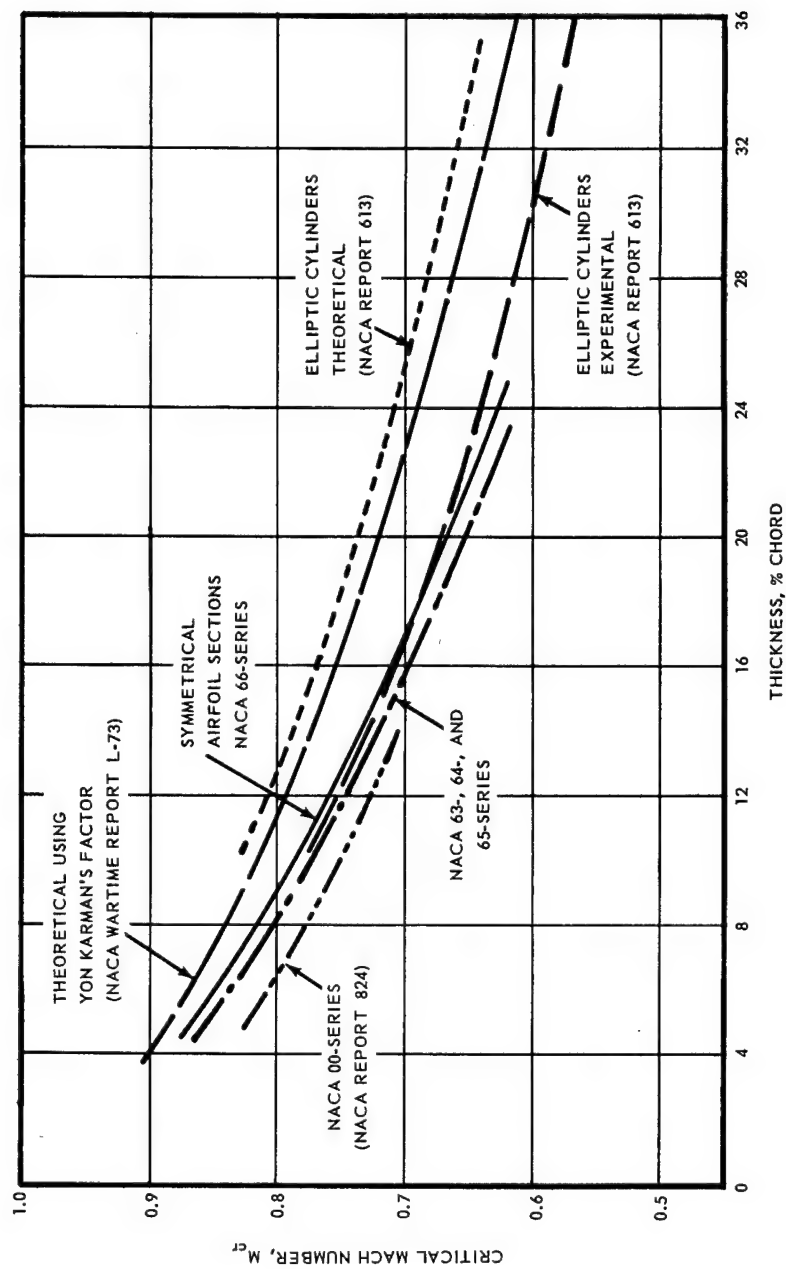
Fig. 15 — Variation of critical Mach number with thickness at zero lift

Miscellaneous Cylindrical Shapes

Figure 16 presents for comparison the variation of drag coefficient with Reynolds number of some selected shapes whose drag characteristics are superior to those of a circular cylinder. In this figure the fineness ratio FR is used instead of thickness ratio. The fineness ratio is the reciprocal of the thickness ratio. The drag and Reynolds number for these bodies can be calculated as follows:

$$D = C_D \frac{\rho V^2}{2} A_F$$

$$Re = \frac{Vc\,\rho}{\mu}$$

Table 10 presents values of the drag coefficient at Reynolds number = 10^5 (except where the lowest test Reynolds number was about 2×10^5) for various shapes tested in Reference 9. Examination of these data indicates that the drag coefficient either remained essentially constant or decreased with an increase of the corner radius ratio and that, in general, the drag coefficient decreases with increasing fineness ratio. It should be noted that some influence of end leakage on the drag measurements of these cylinders was present during testing. It is felt that the data are sufficiently accurate to indicate, at least qualitatively, the changes in drag of the various shapes (ellipses, rectangles, diamonds, and triangles) with corner radius ratio and fineness ratio.
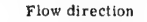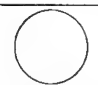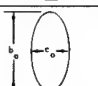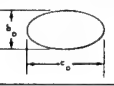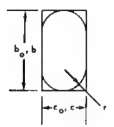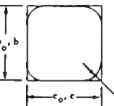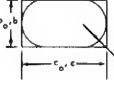
The drag and Reynolds number for these configurations can be calculated using the above equations.

In addition, drag coefficient and Strouhal number are presented in Figures 17 through 23 as a function of Reynolds number for the various shapes listed in Table 10. The Strouhal number is an indication of the frequency of vortex discharge from one side of a body. Accompanying this discharge of vortices from the body is a fluctuation of the pressure in the wake.

Although the Strouhal number data are meager, comparison of Figure 1 and Figures 17 through 23 indicates that at subcritical Reynolds number (Re<10^5) the Strouhal numbers for all shapes were close to 0.2.

At supercritical Reynolds number (Re>10^5) the Strouhal number data presented are for the predominant frequencies encountered, with the exception of the fineness ratio 2:1 rectangle where the disturbances in the wake were periodic and had a value of about 0.4.

39

TABLE 10 GEOMETRIC AND DRAG CHARACTERISTICS OF SELECTED SHAPES
(All dimensions in inches)
(NACA-TN-3038)

Flow direction	Fineness ratio, (c_o/b_o)	Corner-radius ratio, (r/b_o)	Nominal size	b_o	b	c_o	c	r	C_D at $R=10^5$
	1:1	0.50	12	12.00	12.00	12.00	12.00	6.00	
	1:1	0.50	4	4.00	4.00	4.00	4.00	2.00	1.00
	1:1	0.50	1	1.00	1.00	1.00	1.00	0.50	
	1:2	---	12	12.00	12.00	6.00	6.00	---	
	1:2	---	4	4.00	4.00	2.00	2.00	---	1.6
	1:2	---	1	1.00	1.00	0.50	0.50	---	
	2:1	---	12	6.00	6.00	12.00	12.00	---	
	2:1	---	4	2.00	2.00	4.00	4.00	---	0.6
	2:1	---	1	0.50	0.50	1.00	1.00	---	
	1:2	0.021	12	12.00	12.00	6.00	6.00	0.25	
	1:2	0.021	4	4.00	4.00	2.00	2.00	0.08	2.2
	1:2	0.021	1	1.00	1.00	1.50	0.50	0.021	
	1:2	0.083	12	12.00	12.00	6.00	6.00	1.00	1.9
	1:2	0.250	12	12.00	12.00	6.00	6.00	3.00	1.6
	1:2	0.250	4	4.00	4.00	2.00	2.00	1.00	
	1:1	0.021	12	12.00	12.00	12.00	12.00	0.25	
	1:1	0.021	4	4.00	4.00	4.00	4.00	0.08	2.0
	1:1	0.021	1	1.00	1.00	1.00	1.00	0.021	
	1:1	0.167	12	12.00	12.00	12.00	12.00	2.00	1.2[a]
	1:1	0.333	12	12.00	12.00	12.00	12.00	4.00	1.0
	1:1	0.333	1	1.00	1.00	1.00	1.00	0.33	
	2:1	0.042	12	6.00	6.00	12.00	12.00	0.25	
	2:1	0.042	4	2.00	2.00	4.00	4.00	0.08	1.4
	2:1	0.042	1	0.50	0.50	1.00	1.00	0.021	
	2:1	0.167	12	6.00	6.00	12.00	12.00	1.00	0.7[a]
	2:1	0.500	12	6.00	6.00	12.00	12.00	3.00	0.4
	2:1	0.500	4	2.00	2.00	4.00	4.00	1.00	

[a] $R = 2 \times 10^5$

TABLE 10   GEOMETRIC AND DRAG CHARACTERISTICS OF SELECTED SHAPES (Cont.)
(All dimensions in inches)
(NACA-TN-3038)

| Flow direction	Fineness ratio, (c_o/b_o)	Corner-radius ratio, (r/b_o)	Nominal size	b_o	b	c_o	c	r	C_D at $R = 10^5$
	1:2	0.021	12	12.00	11.38	6.00	5.94	0.25	
	1:2	0.021	4	4.00	3.77	2.00	1.98	0.08	1.8
	1:2	0.021	1	1.00	0.95	0.50	0.49	0.021	
	1:2	0.083	12	12.00	9.53	6.00	5.76	1.00	1.7
	1:2	0.167	12	12.00	7.05	6.00	5.53	2.00	
	1:2	0.167	4	4.00	2.35	2.00	1.84	0.67	1.7
	1:1	0.015	12	16.97	16.76	16.76	16.80	0.25	
	1:1	0.015	4	5.66	5.59	5.66	5.59	0.08	1.5
	1:1	0.015	1	1.41	1.39	1.41	1.39	0.021	
	1:1	0.118	12	16.97	15.31	16.97	15.31	2.00	1.5 [a]
	1:1	0.235	12	16.97	13.66	16.97	13.66	4.00	
	1:1	0.235	4	5.66	4.55	5.66	4.55	1.33	1.5
	2:1	0.042	12	6.00	5.94	12.00	11.42	0.25	
	2:1	0.042	4	2.00	1.98	4.00	3.88	0.08	1.1
	2:1	0.042	1	0.50	0.49	1.00	0.96	0.02	
	2:1	0.167	12	6.00	5.76	12.00	9.50	1.00	1.1 [a]
	2:1	0.333	12	6.00	5.53	12.00	7.05	2.00	
	2:1	0.333	4	2.00	1.84	4.00	2.35	0.67	1.1
	1:1	0.021	12	12.00	11.69	12.00	11.69	0.25	
	1:1	0.021	4	4.00	3.90	4.00	3.90	0.08	1.2
	1:1	0.021	1	1.00	0.98	1.00	0.98	0.021	
	1:1	0.083	12	12.00	10.77	12.00	10.77	1.00	1.3 [a]
	1:1	0.250	12	12.00	8.29	12.00	8.29	3.00	
	1:1	0.250	4	4.00	2.78	4.00	2.76	1.00	1.1
	1:1	0.021	12	12.00	11.69	12.00	11.69	0.25	
	1:1	0.021	4	4.00	3.90	4.00	3.90	0.08	2.0
	1:1	0.021	1	1.00	0.98	1.00	0.98	0.021	
	1:1	0.083	12	12.00	10.77	12.00	10.77	1.00	1.9 [a]
	1:1	0.250	12	12.00	8.29	12.00	8.29	3.00	
	1:1	0.250	4	4.00	2.76	4.00	2.76	1.00	1.3

[a] $R = 2 \times 10^5$

42
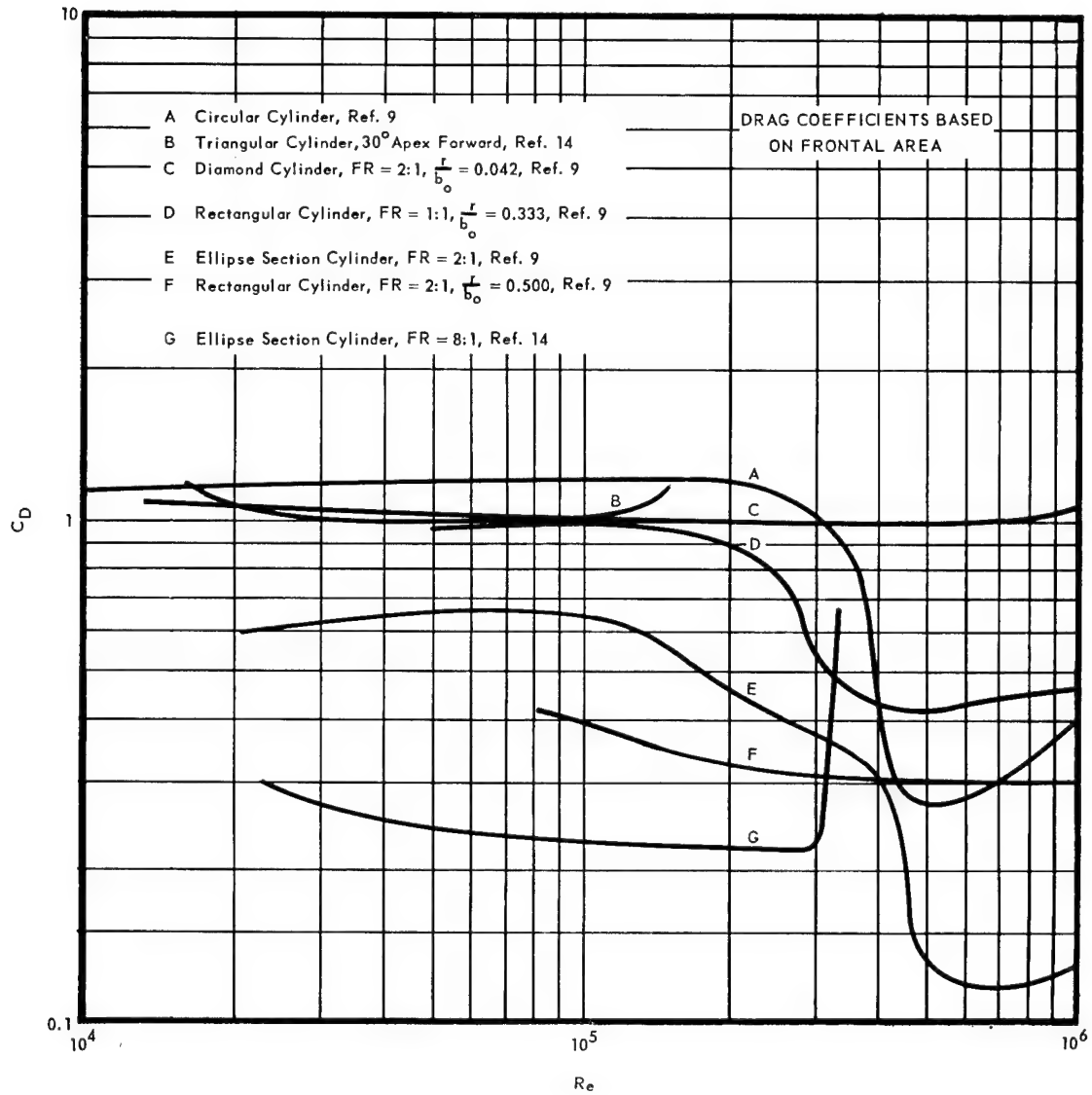
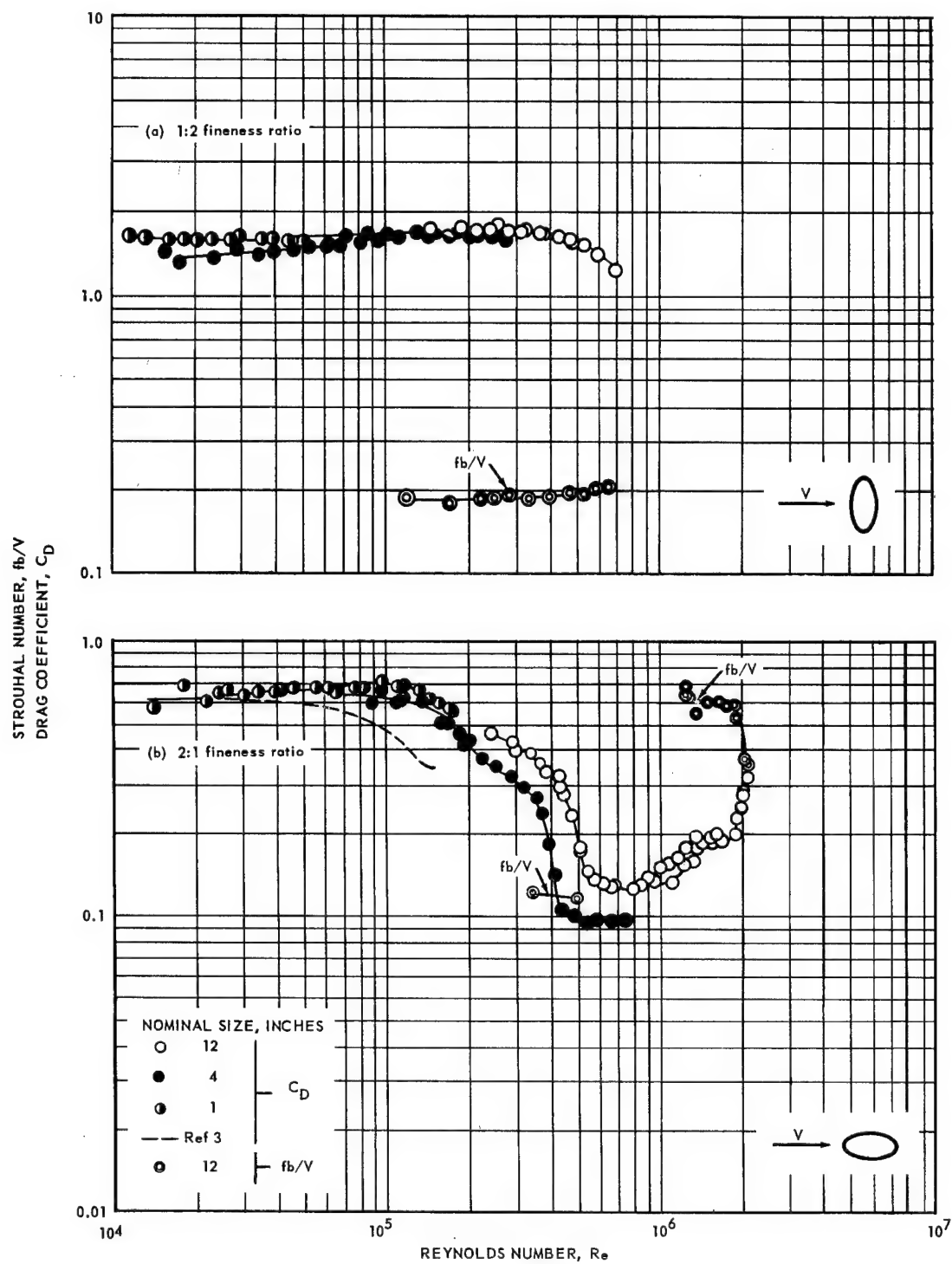Fig. 16—Comparison of drag characteristics of several selected shapes

Fig. 17 — Variation of drag coefficient and Strouhal number with Reynolds number
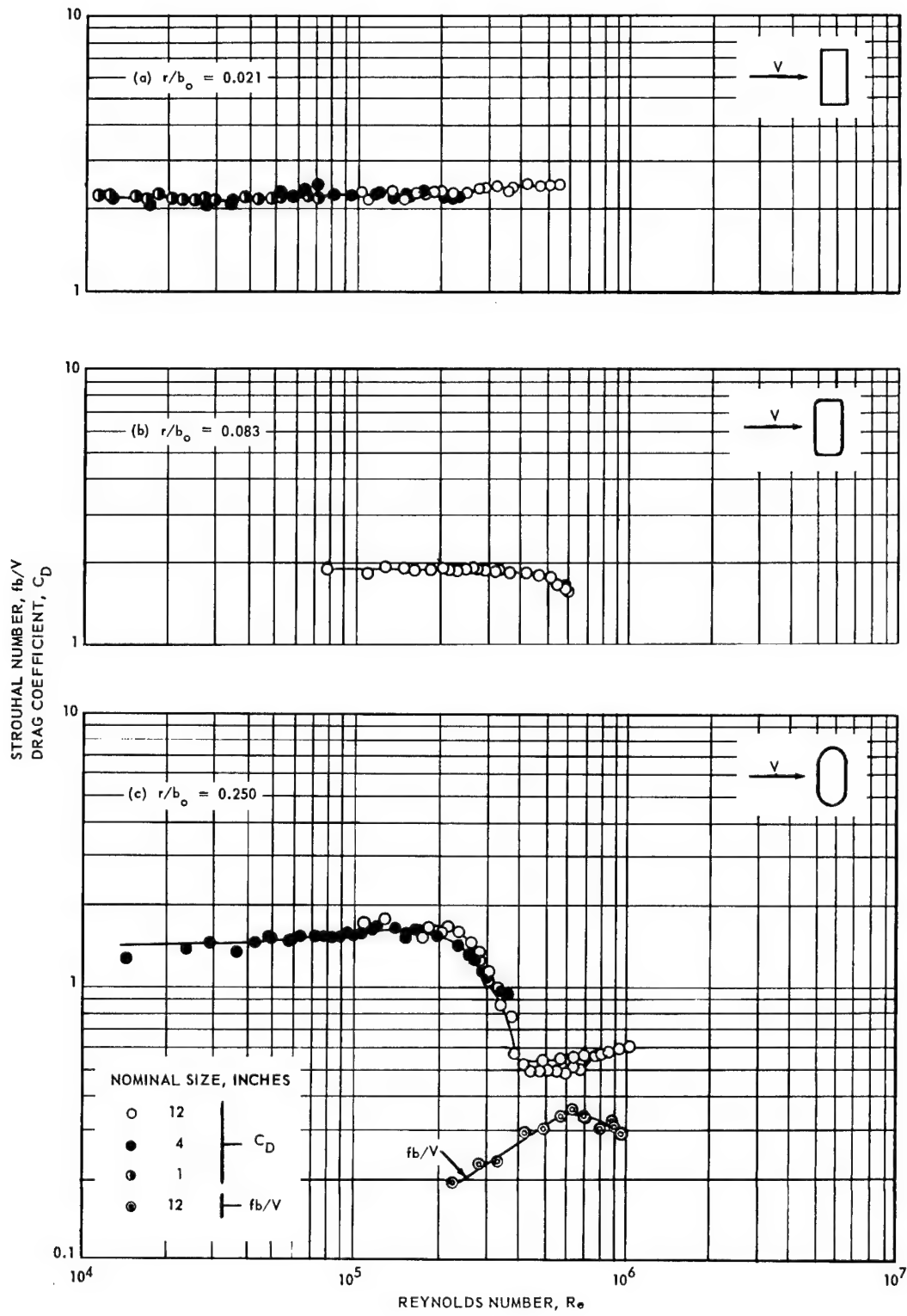for the elliptic cylinders (NACA-TN-3038)

Fig. 18 — Variation of drag coefficient and Strouhal number with Reynolds number for 1:2 fineness ratio rectangular cylinders (NACA-TN-3038)
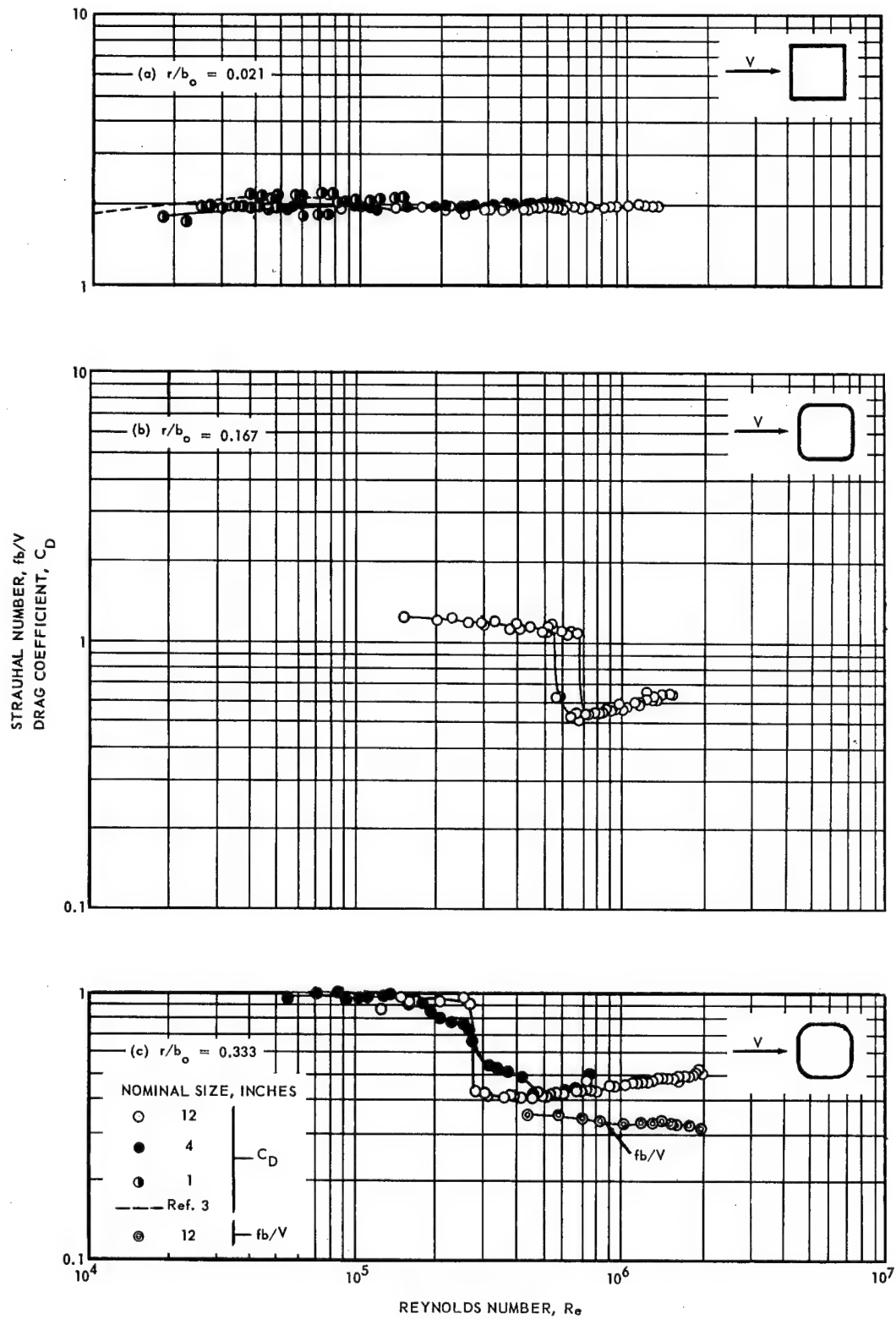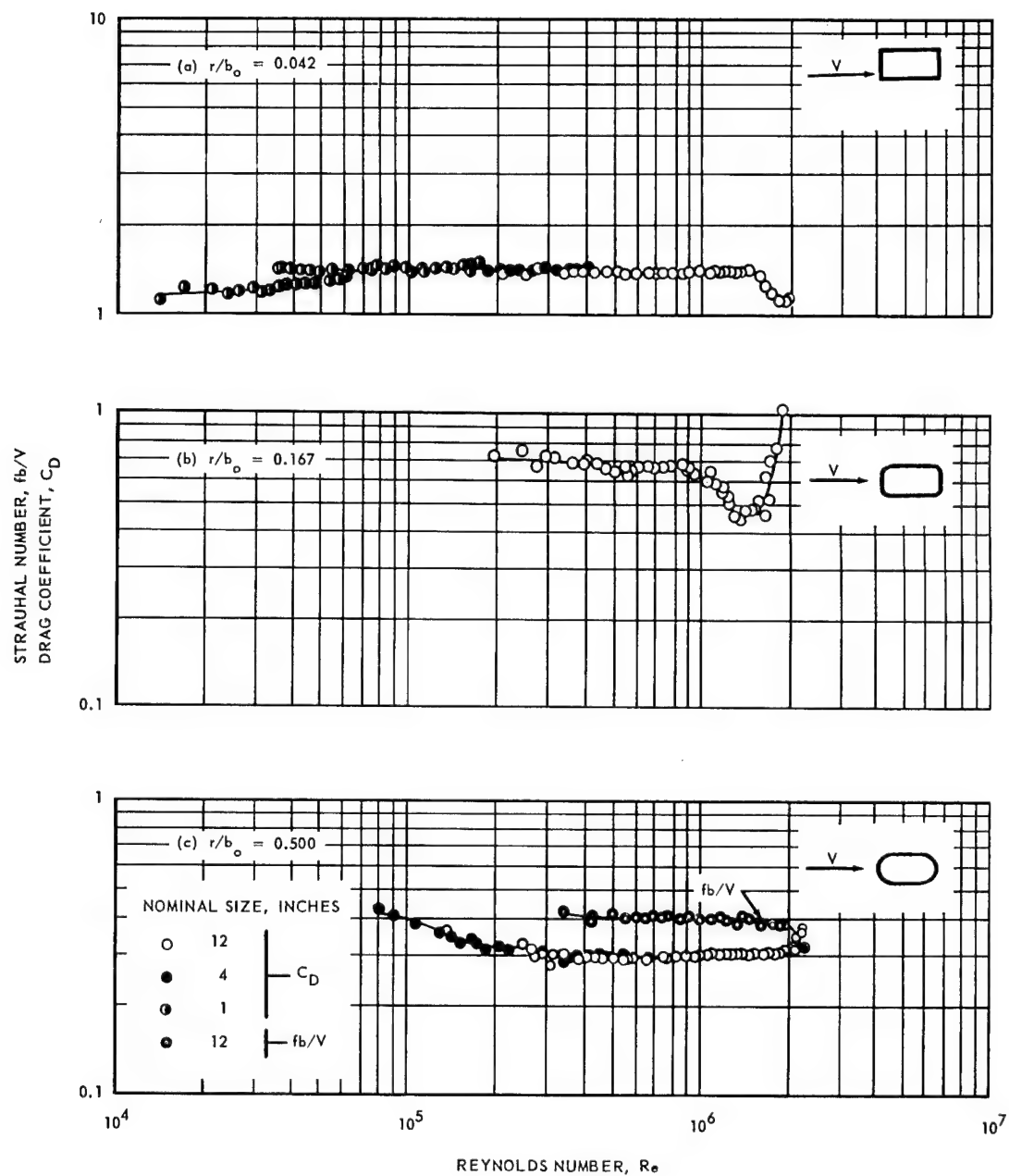
Fig. 19—Variation of drag coefficient and Strouhal number with Reynolds number
for the 1:1 fineness ratio rectangular cylinders (NACA-TN-3038)

Fig. 20 — Variation of drag coefficient and Strouhal number with Reynolds number for the 2:1 fineness ratio rectangular cylinders (NACA-TN-3038)
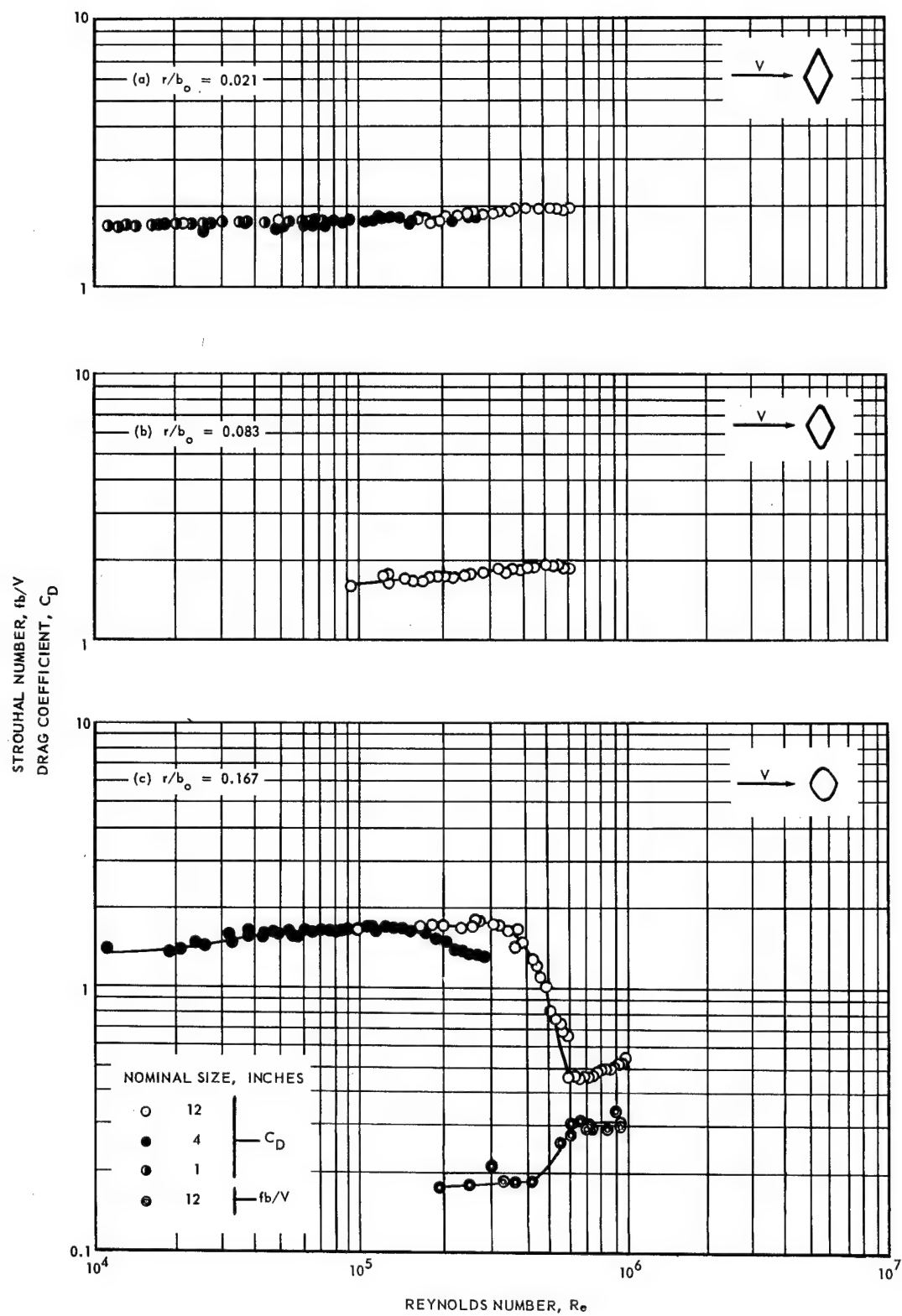
Fig. 21 – Variation of drag coefficient and Strouhal number with Reynolds number
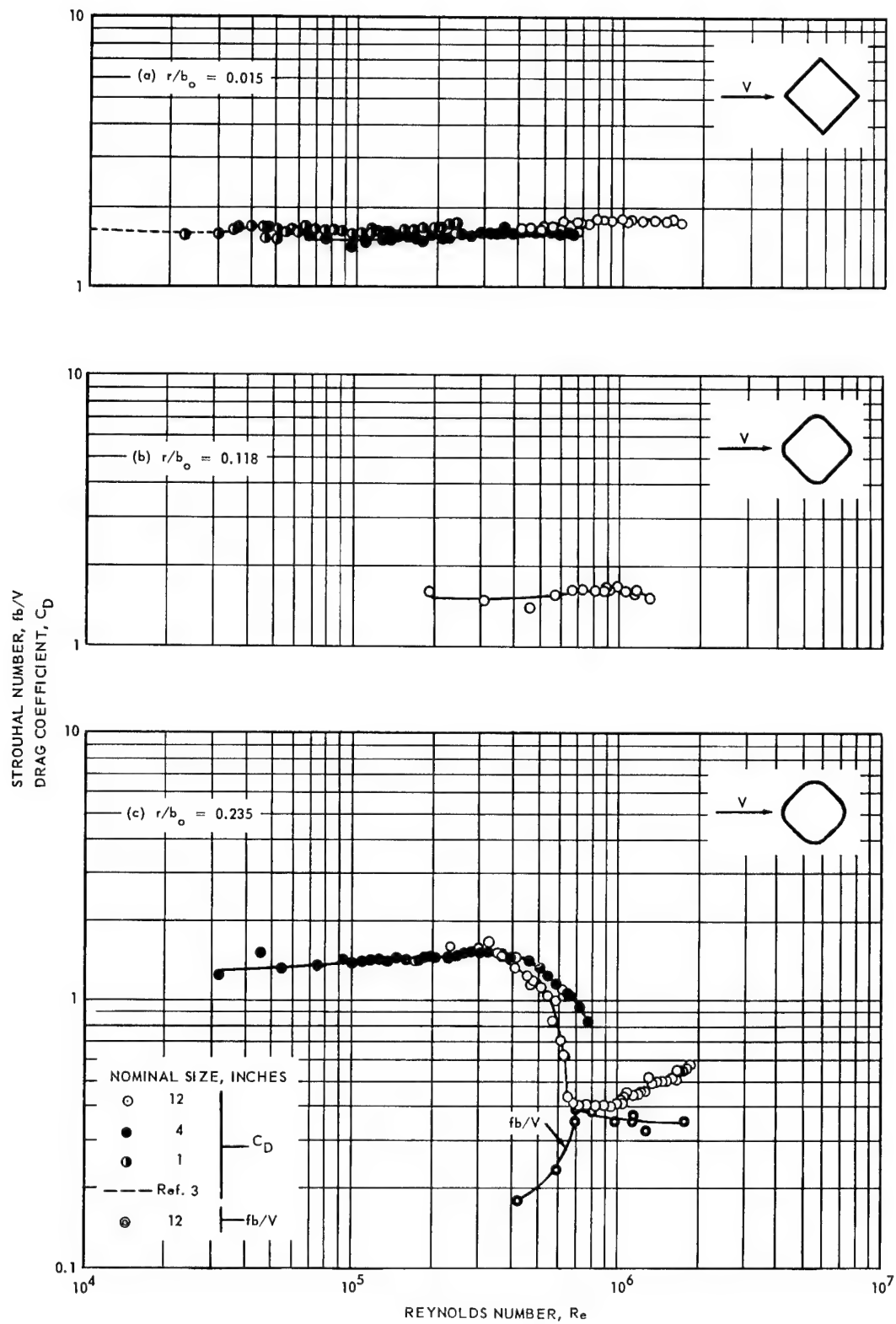for the 1:2 fineness ratio diamond cylinders (NACA-TN-3038)

48

Fig. 22 — Variation of drag coefficient and Strouhal number with Reynolds number
for the 1:1 fineness ratio diamond cylinders (NACA-TN-3038)

Fig. 23 — Variation of drag coefficient and Strouhal number with Reynolds number for the 2:1 fineness ratio diamond cylinders (NACA-TN-3038)
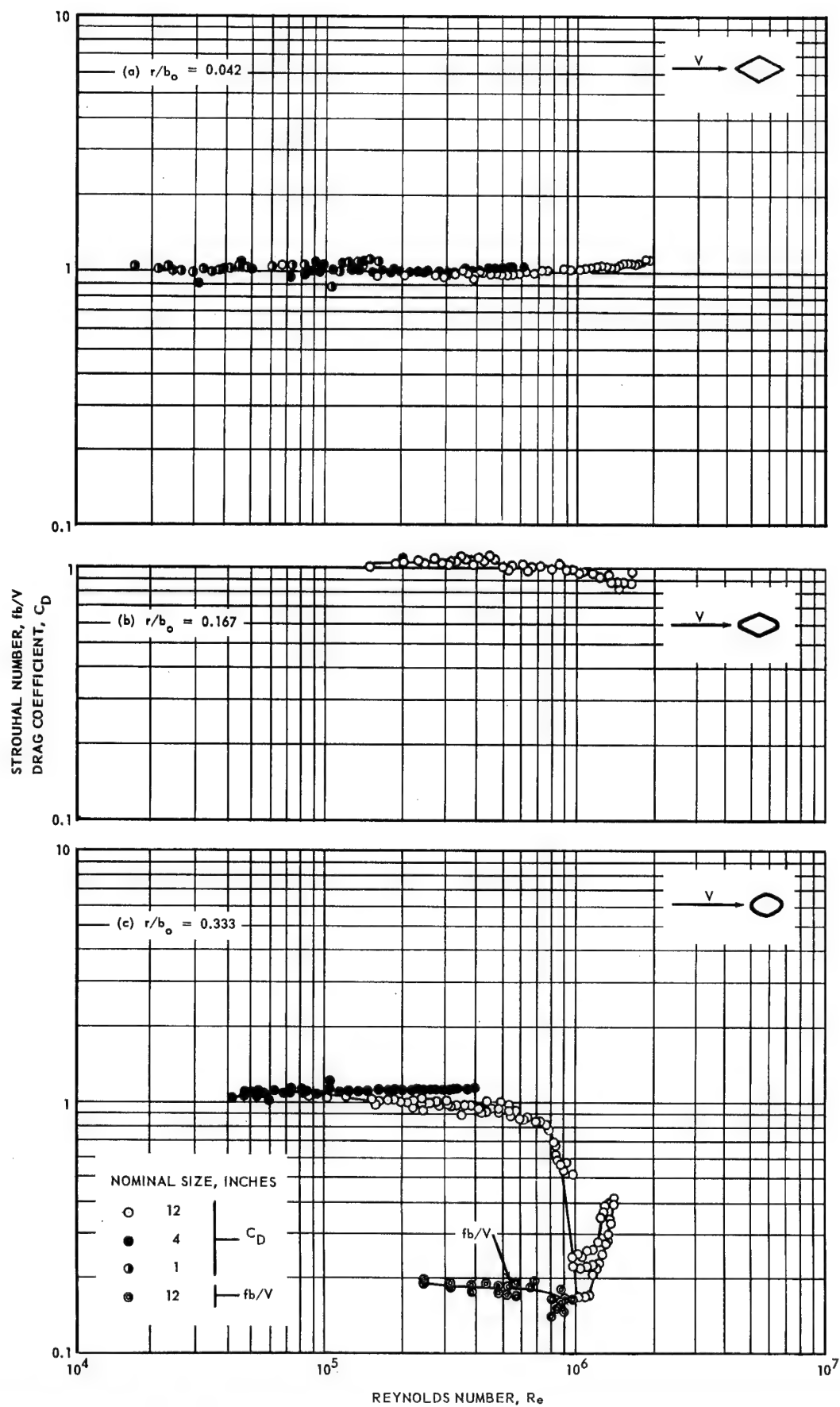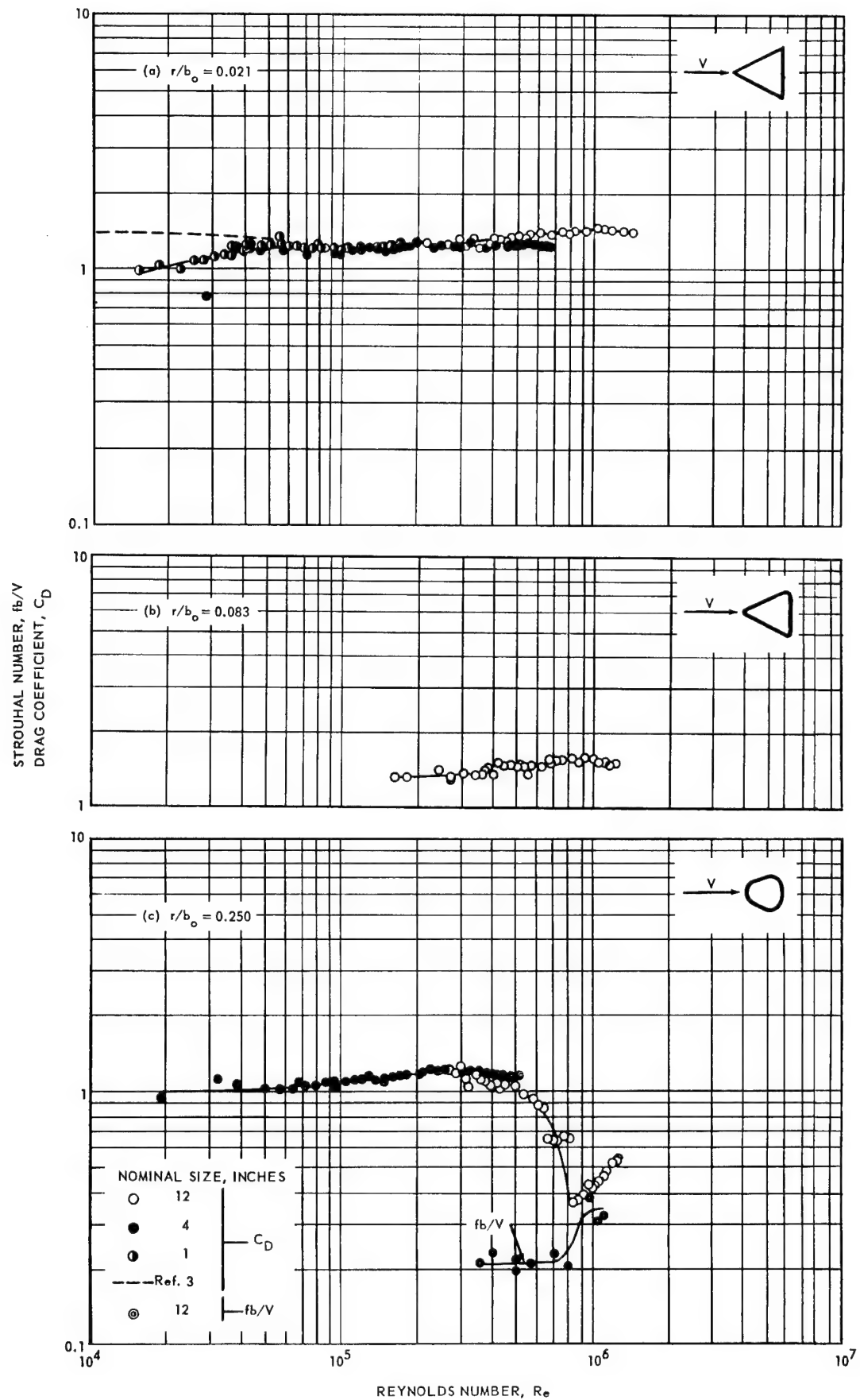
50

Fig. 24 – Variation of drag coefficient and Strouhal number with Reynolds number
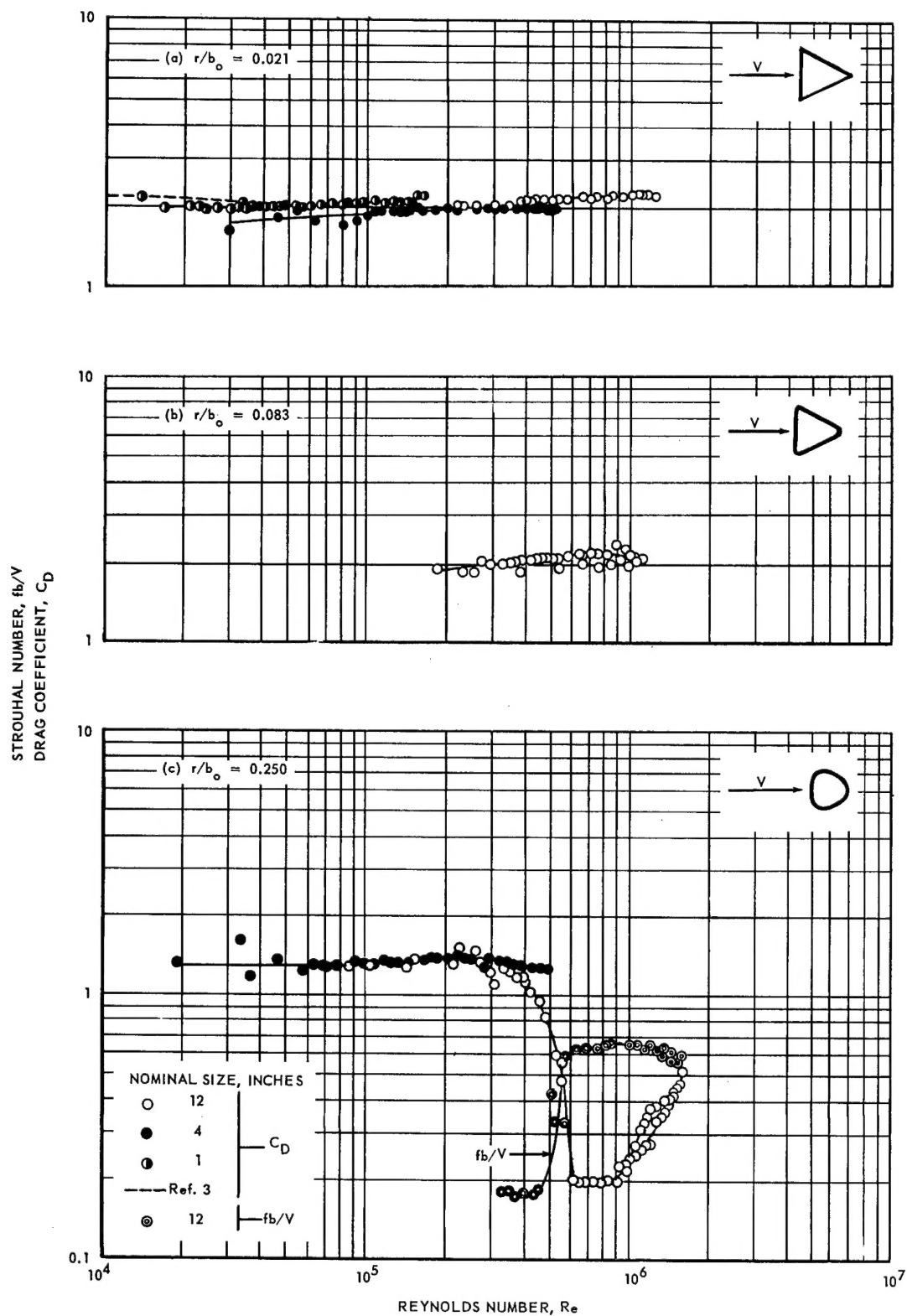for the isosceles triangular cylinders with apex forward (NACA-TN-3038)

Fig. 25 — Variation of drag coefficient and Strouhal number with Reynolds number
for the isosceles triangular cylinders with base forward (NACA-TN-3038)

Appendix
Summary of
Available Literature on Tube Banks

ASME Trans., 76:381 (1954). "Heat Transfer and Friction Characteristics for Flow of Gases Normal to Banks of Tubes - Use of Transient Test Technique."

Transition-region flow across circular tubes in various bank geometries. Results are of interest in applications involving small-diameter tubes and low-density fluids.

ASME Trans., 74:953 (1952). "Heat Transfer and Fluid Friction During Flow Across Banks of Tubes."

Transition-region flow of light oil across banks of tubes of staggered and in-line geometry.

ASME Trans., 67:643 (1945). "A General Correlation of Friction Factors for Various Types of Surfaces in Cross Flow."

Work correlating the effect on the friction coefficient of changing bank geometry. Includes an equation of possible outstanding value.

NACA Wartime Report L-609 (1943). "An Experimental Survey of Flow Across Banks of Elliptical and Pointed Tubes."

Experimental data on pressure drag across banks of elliptical and pointed tubes in various geometry.

AICHE Trans., 29:161 (1933). "Pressure Drop Across Banks of Tubes."

ASME Trans., 59:583 (1937). "Correlation and Utilization of New Data on Flow Resistance and Heat Transfer for Cross Flow of Gases Over Tube Banks."

ASME Trans., 60:381 (1938). "Heat Transfer and Flow Resistance in Cross Flow of Gases over Tube Banks."

ASME Trans., 61:705 (1939). "The Analogy Between Fluid Friction and Heat Transfer."

Stanford University Technical Report No. 23, "Compact Heat Exchangers - A Summary of Basic Heat Transfer and Flow Friction Design Data," W. M. Kays and A. L. London (Nov. 15, 1954).

References

1. ASME Trans., 72:881 (1950). "Heat Transfer and Fluid Friction During Viscous Flow Across Banks of Tubes." (Bergelin, Brown, Hull, and Sullivan).

2. ASME Trans., 76:387 (1954). "Heat Transfer and Friction Coefficient for Flow of Gas Normal to Tube Banks - Use of Transient-Test Technique" (Kays, London, and Lo).

3. ASME Trans., 74:953 (1952). "Heat Transfer and Fluid Friction During Flow Across Banks of Tubes." (Bergelin, Brown, and Doberstein).

4. ASME Trans., 74:1167 (1952). "Heat Transfer and Flow Friction Characteristics of Some Compact-Heat-Exchanger Surfaces." (London, Kays, and Johnson).

5. "Heat Transmission" (1954). (McAdams).

6. "Fluid Dynamics and Heat Transfer" (1953). (Knudsen and Katz).

7. "Modern Developments in Fluid Dynamics." (1938). Volumes I and II (Goldstein).

8. Ind. and Engr. Chem., 30:942 (1938). "Heat Transfer Coefficient in Staggered Tube Banks." (Winding).

9. NACA-TN-3038 (1953). "Low Speed Drag of Cylinders of Various Shapes." (Delany and Sorensen).

10. NACA Wartime Report L-232 (1942). "An Experimental Investigation of Flow Across Tube Banks." (Brevoort and Tifford).

11. NACA Wartime Report L-609 (1943). "An Experimental Survey of Flow Across Banks of Elliptical and Pointed Tubes." (Joynes and Palmer).

12. ASME Trans. 67:643 (1945). "A General Correlation of Friction Factors for Various Types of Surfaces in Cross Flow." (Gunter and Shaw)

13. ASME Trans., 71:396 (1949). "A Study of Three Tube Arrangements in Unbaffled Tubular Heat Exchangers." (Bergelin et al).

14. NACA Report 619 (1937). "Drag of Cylinders of Simple Shapes." (Lindsey).

15. "Mechanical Similitude and Turbulence." (von Karman).

16. NACA Report 586 (1937). "Airfoil Section Characteristics as Affected by Variations of the Reynolds Number." (Jackobs and Sherman).

17. NACA Report 824 (1945). "Summary of Airfoil Data." (Abbot, von Doenhoff, and Stivers).

18. NACA Wartime Report L-781 (1940). "Estimation of Critical Speeds of Airfoils and Streamline Bodies." (Robinson and Wright).

19. Kent's Mechanical Engineers' Handbook, Power Volume (1950). Parasite Resistance. (Teichmann).

20. AGT Design Data Standard.

21. NACA Report 311 (1929). "Aerodynamic Theory and Test of Strut Forms." (R. H. Smith).

22. NACA Report 335 (1929). "Aerodynamic Theory and Test of Strut Forms - II." (R. H. Smith)

23. NACA Report 289 (1928). "Forces on Elliptic Cylinders in Uniform Air Stream." (A. F. Zahm, R. H. Smith, F. A. Lauden)

24. Reports and Memoranda No. 1241 (1929). "Experiments on a Series of Symmetrical Joukowski Sections." (A. Foge, V. M. Falkner, W. S. Walker) British

25. Reports and Memoranda No. 1327 (1930). "Wind Tunnel Tests of Seven Struts." (A. S. Hartshorn) British.

26. Reports and Memoranda No. 1599 (1934). "Resistance of Certain Strut Forms." (R. Warden) British

27. "Aerodynamic Drag" Sighard F. Horner, The Otterbein Press, 1951